**Australian Government**
**Department of Defence**
Defence Science and
Technology Organisation

# Principles and Application of Magnetic Rubber Testing for Crack Detection in High-Strength Steel Components: I. Active-Field Inspection

*S K Burke, M E Ibrahim and G R Hugo*

**Maritime Division**
Defence Science and Technology Organisation

DSTO-TR-3032

## ABSTRACT

Magnetic rubber testing (MRT) is a sensitive non-destructive inspection technique, capable of detecting cracks as small as 0.5 mm (0.020 inch) in length with high reliability. Since its introduction in the 1970s, MRT has been successfully used to inspect high-strength steel aerospace components for surface-breaking fatigue cracks. However, despite its widespread use and apparent simplicity, the underpinning science of MRT is not highly developed. In response to some uncertainties regarding potential unreliability in the application of MRT for certain test conditions, the scientific principles governing both active-field and residual-field variants of MRT were examined. The results of theoretical and experimental investigations into active-field MRT are documented in the current report, which describes the principles of active-field MRT, and then examines both the basis for verification of adequate applied field strength for D6ac steel and the effect of the perpendicular versus tangential components of applied magnetic field on inspection reliability. The results of related study into residual-field MRT are presented in a companion DSTO report.

**RELEASE LIMITATION**

*Approved for public release*

**APPROVED FOR PUBLIC RELEASE**

# Principles and Application of Magnetic Rubber Testing for Crack Detection in High-Strength Steel Components: I. Active-Field Inspection

## Executive Summary

Magnetic Rubber Testing (MRT) is a sensitive non-destructive inspection technique that has been applied to the detection of fatigue cracks in high-strength steel components since the late 1970s. MRT is typically called upon to reliably detect cracks as small as 0.5 mm (0.020 inch) in length.

Historically, MRT found its most extensive application in the inspection of critical high-strength steel components of the F-111 aircraft to ensure their continued structural airworthiness. The Royal Australian Air Force was sole operator of the F-111 from 1998–2010. During this period the Defence Science and Technology Organisation (DSTO) conducted a range of studies into the underpinning science and application of MRT to high-strength D6ac steel, stimulated by concerns about potential unreliability of MRT under some test conditions. The aim of the present report is make the results of this body of work available to the broader non-destructive testing community, both to improve the practice of MRT as well as to stimulate further research into this useful technique.

The process of MRT is deceptively simple. It involves the application of a liquid silicone rubber containing a dispersion of ferromagnetic particles to the surface of a magnetised steel component. Following curing of the rubber, any surface-breaking cracks present in the component are revealed on the surface of the rubber cast by distinct lines of black ferromagnetic particles. These crack indications are formed by the action of the magnetic leakage fields emanating from the component at the crack locations while the liquid rubber cured. There are two main variants of MRT: (i) active field MRT, in which an external magnetic field is applied to the component while the rubber cures, and (ii) residual field MRT, which utilises the residual (or remanent) magnetisation remaining in the component following prior magnetisation by an external magnetic field before the rubber is applied.

The contents of the report are as follows. First, the background and theory of MRT derived from a critical review of the literature are presented, together with a summary of the magnetic properties of D6ac steel. The basis for adequate verification of field strength in active-field MRT of D6ac is then examined followed by an investigation of the effect of perpendicular versus tangential components of magnetic field on defect detectability. Here the results of an experimental study are used to estimate the reduction in the sensitivity of active-field MRT as a function of perpendicular and tangential field strength. Finally, the physical characteristics of magnetic rubber (rubber viscosity and magnetic particle properties) are included for completeness.

The results of related investigations into residual-field MRT are documented in the companion report, DSTO-TR-3033.

# Authors

## S K Burke
Maritime Division

*Steve Burke is Group Leader Acoustic Material Systems within Maritime Division and Task Leader for AIR 07/101 Assessment and Control of Aircraft Materials Degradation. His association with electromagnetic nondestructive evaluation research spans several decades. He was awarded a BSc (Hons) from Monash University, and a PhD from Imperial College, London. Steve is a Fellow of the Australian Institute of Physics and a Chartered Physicist.*

_____     _____

## M E Ibrahim
Maritime Division

*Matthew Ibrahim holds a BSc in physics and materials science, and an MSc in theoretical and experimental NDE from Monash University. He has performed NDE research in ultrasonic and electromagnetic NDE at DSTO since 1998, and is currently the Science Team Leader for NDE Research for air platforms under task AIR 07/101.*

_____     _____

## G R Hugo
Maritime Division

*Geoff Hugo is Group Leader Corrosion Science within Maritime Division. He has previously led research programs in advanced electromagnetic and ultrasonic NDE for aircraft applications. Geoff has BSc and BE degrees, and a PhD from Monash University, and is the Australian National Leader for The Technical Cooperation Program Materials Group Technical Panel on Nondestructive Characterisation and Materials State Awareness.*

_____     _____

*This page is intentionally blank*

# Contents

# Abbreviations

| | |
|---|---|
| AC | Alternating current |
| ADF | Australian Defence Force |
| CGS | Centimetre Gram Second electromagnetic measurement units |
| DC | Direct current |
| DGTA-ADF | Directorate General Technical Airworthiness – ADF |
| DSTO | Defence Science and Technology Organisation |
| D6ac | Denotes a grade of high strength steel |
| MLE | Maximum likelihood estimate |
| MPI | Magnetic particle inspection |
| MRT | Magnetic rubber testing |
| NDE | Nondestructive evaluation |
| NDI | Nondestructive inspection |
| NDT | Nondestructive testing |
| NDT&CT | Nondestructive Testing and Composite Technology (within DGTA-ADF) |
| POD | Probability of detection (of a crack) |
| RAAF | Royal Australian Air Force |
| UHS | Ultra-high strength |

# Symbols

| | |
|---|---|
| $a_{90}$ | Surface crack length for which the POD is 90% |
| $a_{50/95}$ | Surface crack length for which a POD of 90% has been demonstrated with 95% statistical confidence |
| $a_{\mathrm{NDI}}$ | Length of the smallest crack that can be reliably detected |
| $\boldsymbol{B}$ | Magnetic induction, Magnetic flux density |
| $B$ | Magnitude of magnetic induction $= |\mathbf{B}|$ |
| $B_n$ | Component of $\mathbf{B}$ normal (perpendicular) to the surface of a material |
| $\boldsymbol{B_r}$ | Remanent magnetic induction (Remanence) |
| $B_t$ | Component of $\mathbf{B}$ tangent (parallel) to the surface of a material |
| $\boldsymbol{F}$ | Magnetic force on a particle |

| | |
|---|---|
| $\phi*$ | Magnetic scalar potential |
| $\boldsymbol{H}$ | Magnetic field strength, Magnetising force |
| $H$ | Magnitude of magnetic field strength = $|\boldsymbol{H}|$ |
| $\boldsymbol{H}_c$ | Coercive field |
| $H_n$ | Component of $\mathbf{H}$ normal (perpendicular) to the surface of a material |
| $H_{max}$ | Maximum excursions of $H$ for a minor hysteresis loop |
| $H_t$ | Component of $\mathbf{H}$ tangent (parallel) to the surface of a material |
| $\mu_r$ | Relative magnetic permeability |
| $\mu'_r$ | Differential relative magnetic permeability |
| $\mu_0$ | Permeability of free space |
| $\boldsymbol{M}$ | Magnetisation |
| $\boldsymbol{M_p}$ | Magnetisation of a particle |
| $\rho*$ | Surface magnetic pole density |
| $\sigma$ | Volume magnetic pole density |
| $t_{PL}$ | Magnetic rubber pot life |
| $V$ | Volume of a magnetic particle |

*This page is intentionally blank*

# 1. Introduction

When the F-111 tactical strike aircraft was introduced into service in 1967 it brought with it the extensive use of a new ultra high strength (UHS) steel designated D6ac, which comprised the majority of fracture critical components of the airframe [1]. However, within a short period of usage, it became clear that cyclic loading of the steel resulted in fatigue failures with extremely short critical crack lengths, resulting in catastrophic failure of a wing pivot fitting as early as 1969 [2].

In order to provide a means of detecting very small surface-breaking cracks, General Dynamics, the manufacturer of the F-111, developed and patented a liquid rubber inspection method, in which magnetic particles suspended in the rubber would be drawn to crack locations in the surface of a magnetised component via magnetic flux leakage [3, 4]. Magnetic Rubber Testing (MRT) became a staple nondestructive inspection (NDI) method for the detection of small fatigue cracks in D6ac steel components of the F-111. A particular advantage of MRT was the distinct and permanent records that could be produced and retained for subsequent examination and for comparison with future inspection results.

With many years' experience, MRT evolved into a highly reliable and sensitive technique, generally capable of detecting cracks as small as 0.5 mm (0.020 inch)* in length in steel components. For certain inspections, defect probability of detection trials have demonstrated that MRT could be used to detect cracks reliably down to 0.3 mm (0.012 inch) in length [5, 6].

During the 30+ year period of operation of the F-111, increasingly stringent expectations concerning acceptable levels of engineering risk coincided with advances in the science underpinning the application of NDI techniques to ensure aircraft structural integrity. Consequently, despite the apparent maturity of MRT, a number of uncertainties were identified regarding the reliability of MRT for crack detection. As a result, DSTO undertook a substantial research program examining various aspects of the application of MRT to D6ac steel. The results of this program were progressively communicated to RAAF airworthiness authority (Directorate General of Technical Airworthiness, DGTA) and the F-111 maintenance community via an ongoing series of DSTO technical reports [7 - 10], as well as numerous DSTO client reports, internal minutes and memoranda throughout the period 2005 to 2009.

The aim of the present report and its companion [11] is to draw together the results of these investigations into a more accessible reference and to make the results of this body of work available to the broader NDT community, to both improve the practice of MRT and stimulate further research into this sensitive technique.

In this report, the background theory for MRT distilled from a critical review of the available literature is presented in Section 2 together with a summary of the magnetic

---

* Imperial units (1inch=25.4 mm) for crack length: included for the sake of consistency with then F-111 practice.

properties of the UHS D6ac steel used in the F–111 aircraft. The basis for adequate verification of field strength in active-field MRT of D6ac is outlined in Section 3. The effect of normal versus tangential components of magnetic field on defect detectability is then discussed in Section 4, which includes the results of an experimental study to estimate the reduction in the reliability of active-field MRT as a function of different ratios of normal to tangential field strength. The effect of magnetisation duration is briefly considered in Section 5. For completeness, the physical characteristics of magnetic rubber (rubber viscosity and magnetic particle properties) are included in Section 6.

A companion report, DSTO-TR-3033 [11], describes a related investigation into MRT performed using residual magnetic fields.

# 2. Background

## 2.1 Overview of magnetic rubber testing

Like other magnetic inspection techniques, MRT relies on the leakage of magnetic flux in the vicinity of a discontinuity in a ferromagnetic material to detect structural flaws such as fatigue cracks or fabrication defects.

For inspection of UHS steel components, a liquid silicone rubber containing a suspension of fine magnetic particles is poured onto the steel surface over a potential crack location and the rubber is allowed to cure. If a surface-breaking crack is present, magnetic particles in the liquid rubber are attracted to the mouth of the crack (due to the magnetic leakage flux, Figure 1) where they accumulate producing a crack 'indication'. As the rubber cures, its viscosity increases and so the mobility of the magnetic particles decreases until eventually the particles become fixed in position in the now solid rubber providing a permanent crack indication on the surface of the cured rubber. Once the rubber has fully cured to have sufficient mechanical strength, the rubber 'cast' is removed from the component and examined under a low-power optical microscope for dark crack indications on the surface of the rubber which had been in contact with the steel surface [12]. An example of an MRT crack indication is shown in Figure 2, where the concentration of black particles along the crack is clearly visible against the lighter pigments of the silicone rubber base.
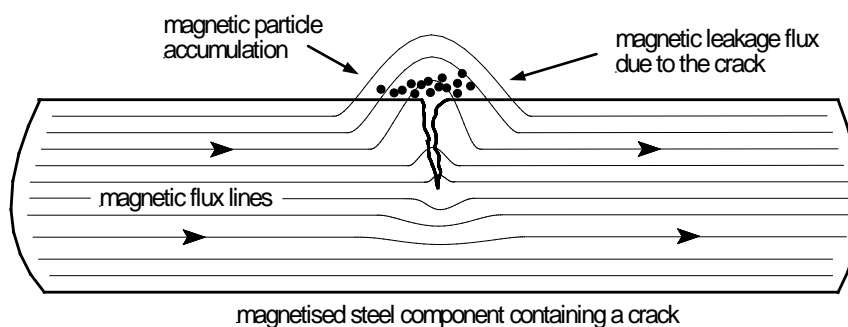


*Figure 1.    Schematic diagram showing the magnetic rubber testing process*
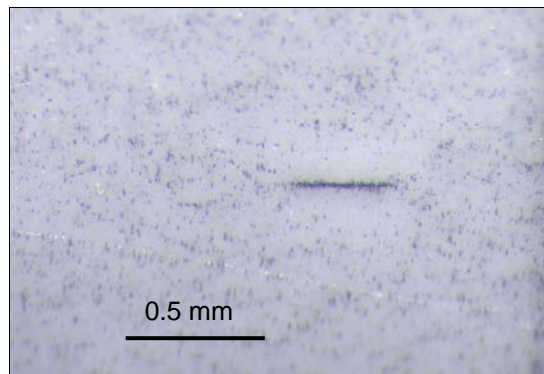
0.5 mm

*Figure 2.   MRT indication of a fatigue crack of surface length 0.35 mm in a D6ac steel test standard (residual-field inspection)*

Two main variants of practical MRT are distinguished by the nature of the magnetic field employed in the inspection as follows:

- *Active-* or *continuous field MRT*. An externally applied magnetic field is applied to the component by a permanent magnet or DC electromagnet and maintained whilst the rubber cures.

- *Residual-field MRT*. An external magnetic field is applied to the structure and then removed. The rubber is subsequently applied to the component and allowed to cure while the specimen is in a remanent magnetic state.

*Central conductor MRT* is a variant of the residual-field technique used for the inspection of fastener or attachment holes. The external field is applied by passing a large (~ 1 kA) pulsed DC current through a conductor inserted centrally through the hole. On removal of the field, a circumferential residual magnetisation is retained within the material immediately surrounding the hole.

For optimum crack detection using MRT, simple geometry dictates that the local magnetisation of the specimen should be perpendicular to the face of the crack in order to generate the largest leakage fields [12].

## 2.2  Theory

There is very little published work on the fundamental theory or practice of MRT. However, it is possible to draw on the considerable body of research literature for the related techniques of magnetic particle inspection (MPI) and magnetic flux leakage and thereby develop the theoretical background for magnetic rubber testing [13-19].

Despite the apparent simplicity of practical MRT, the underlying science is complex. The fundamental concept can be expressed through a single equation, Eq. (1), which relates the magnetic force $F$ acting on an idealised spherical magnetic particle to the magnetic field strength $H$ at the particle position [16, 20, 21]:

$$F = \frac{1}{2}\mu_0 \, V \, \nabla(\boldsymbol{M}_p \cdot \boldsymbol{H}) \, , \tag{1}$$

where $V$ is the particle volume, $\mu_0$ is the permeability of free space and $\boldsymbol{M}_p$ is the particle magnetisation. For a spherical particle with large magnetic permeability it can be shown that $\boldsymbol{M}_p \approx 2\boldsymbol{H}$ and Eq. (1) reduces to the form [21]

$$\begin{aligned}\boldsymbol{F} &= \mu_0 \, V \, \nabla(\boldsymbol{H} \cdot \boldsymbol{H}) \\ &= 2\mu_0 \, V \, |\boldsymbol{H}| \nabla(|\boldsymbol{H}|) \, .\end{aligned} \tag{2}$$

Thus, from Eq. (2), the force on the particle depends on the product of the magnetic field and the magnetic field gradients. It follows that in a uniform magnetic field the force on the particle will actually be zero, because the magnetic field gradient is zero. The fundamental MRT mechanism works only because of the attractive force produced by the gradients in the leakage field in the vicinity of a crack in a magnetised component.

Even in the absence of eddy-current effects, the calculation of the magnetic leakage field and field gradients in the vicinity of a crack required in Eq. (2) is a challenging magnetostatics problem. The conventional formalism for describing the leakage field in the nondestructive evaluation (NDE) literature is rather idiosyncratic, in the sense that it draws on a mathematical analogy with electrostatics and represents the field in terms of magnetic poles or 'charges'. According to this formalism [22, 23], the magnetic field in a region free of conduction currents can be expressed in terms of a magnetic scalar potential $\phi*$ via

$$\boldsymbol{H} = -\nabla \phi* \, , \tag{3}$$

where $\phi*$ satisfies the Poisson equation

$$\nabla^2 \phi* = -\rho* \, , \tag{4}$$

and $\rho*$ is an effective magnetic charge density related to the magnetisation $\boldsymbol{M}$ at any point according to

$$\rho* = -\nabla \cdot \boldsymbol{M} \, . \tag{5}$$

The magnetic scalar potential at a point $(x', y', z')$ outside a magnetic body containing a crack can then be represented in terms of the 'volume' charge density $\rho*$ within the volume $V_M$ of the body and the 'surface' magnetic charge density $\sigma$ on the surfaces $S_M$ of the body and the crack through the general expression

$$\phi*(x', y', z') = \frac{1}{4\pi}\int_{V_M} \frac{\rho*(x,y,z)}{r}\,\mathrm{d}V + \frac{1}{4\pi}\int_{S_M} \frac{\sigma(x,y,z)}{r}\,\mathrm{d}S \, , \tag{6}$$

with the surface pole density given by

$$\sigma = \hat{\boldsymbol{n}} \cdot \boldsymbol{M} \tag{7}$$

where $\hat{\boldsymbol{n}}$ is the unit outward normal to the surface. Here the source coordinates $(x, y, z)$ lie within the volume $V_M$ of the magnetised body and $r^2 = (x - x')^2 + (y - y')^2 + (z - z')^2$.

The early models for magnetic flux leakage from a surface-breaking defect were based on a linear magnetic theory in which the relative permeability $\mu_r$ of the steel was taken to be a constant, i.e. independent of the applied magnetic field. With this assumption, the leakage field can be represented using just a surface distribution of magnetic poles $\sigma$ (or 'surface charges') because the volume charge density $\rho^*$ in Eq. (5) is zero for a linear magnetic material[*]. In the first of such models, Zatsepin and Shcherbinin [24] used a uniform distribution of magnetic poles to describe the leakage field from a 2-D rectangular slot with good success. The major limitation of the work was that the model did not attempt to relate the strength of the leakage field to the applied field strength or the magnetic properties of the steel.

Förster [25], an important contributor to the modern development of magnetic inspection techniques, also examined the leakage field for 2-D cracks with finite and infinite depth using conformal mapping techniques, and attempted to relate the surface change $\sigma$ to the applied magnetic field and magnetic permeability in the special case of a through-thickness crack in a steel pipeline. Sponder *et al.* [26] demonstrated empirically that the shape of the leakage fields predicted by Förster closely approximated experimental observations for fatigue cracks in D6ac under applied loads.

In a significant publication, Edwards and Palmer [21] extended this work and presented an analytical model for the leakage field due to a slot in a thick plate in terms of the applied magnetic field and magnetic permeability. The model was tested by comparison with experimental measurements of the leakage fields for a range of artificial cracks. Edwards and Palmer also estimated the forces experienced by magnetic particles and inferred the field strengths required to detect surface-breaking defects.

In these early models, the surface charge density $\sigma$ was taken to be constant over the faces of the defect. This assumption was subsequently shown to be incorrect if $\sigma$ is calculated self-consistently using the usual integral-equation techniques of potential theory [27]. In fact, a model with constant $\sigma$ is only physically possible in the case of the non-linear theory. The linear theory for magnetic leakage fields continues to be explored using more sophisticated mathematical methods [28-30] and has recently been extended to more complicated geometries, such as flat-bottomed holes and grooves [31], and finite-length rectangular slots in a plate of finite-thickness [32].

While the linear theory for magnetic flux leakage is a good approximation for saturating fields and gives reasonable agreement with experimental results, it is incomplete. For most steels, including D6ac, the magnetic permeability is clearly a non-linear function of applied

---

[*] The volume magnetic charge density is zero for a linear material because in this case $\boldsymbol{M}$ is proportional to $\boldsymbol{B}$ and so $\rho^* = - \text{div } \boldsymbol{M} \propto \text{div } \boldsymbol{B} = 0$ as div $\boldsymbol{B} = 0$ from Maxwell's equations. The volume charge density is also zero for the case of uniform magnetisation $\rho^* = - \text{div } \boldsymbol{M} = 0$ because the divergence of a constant vector is 0.

field, so that the volume charge density $\rho^*$ is non-zero [33] and needs to be taken into account in computing the leakage flux due to a defect according to Eqs (3)–(7). Furthermore, a non-linear theory is required in order to describe flux leakage due to residual magnetisation. Non-linear models with varying levels of complexity have subsequently been developed to describe the flux leakage from surface-breaking defects [27, 33-35], sub-surface defects [36] and defects in residual fields [37, 38].

An alternate approach to modelling of magnetic leakage fields in NDE is to employ numerical procedures such as electromagnetic finite-element [17, 39], finite-difference [40] or boundary-element methods. The feasibility of using finite-element methods to support the development of MRT inspection procedures is discussed in the companion report [11].

If the magnetic leakage fields are known, a simplified quantitative model for the formation of defect indications in MRT can be developed by considering the magnetic, gravitational, convective, thermal and viscous forces acting on the particle. McCoy and Tanner [41, 42] used such an approach to study the effect of magnetic field strength, carrier viscosity and defect aspect ratio on the formation of indications in MPI using computer simulations to solve the equations of motion and obtain the particle trajectories. To represent magnetic rubber, the viscosity of the medium in which the particles are suspended must be time-dependent and increase with time so as to model the curing kinetics of the rubber. The effect of inter-particle interactions has been ignored in models of MPI developed to date, but should be taken into account in the development of any complete theory for MRT [43]. Such effects are obviously present, as shown by the tendency for magnetic particles to chain together in MRT casts, and play an important role in the mechanism of crack indication formation in MPI [43].

In summary, the literature review reveals a broad but incomplete theoretical background underpinning MRT. While the fundamental principles are largely well developed, they have not been combined to form a validated model suitable for predicting the performance of practical MRT.

Irrespective of the status of theoretical models, a prerequisite for successful understanding of MRT is a detailed knowledge of the magnetic properties of the steel under consideration. In the following section, a summary of the magnetic properties of D6ac steel is presented, together with a discussion on the relationships which link measurements of magnetic field outside the component to the fields existing within the steel.

## 2.3 Magnetic properties of D6ac steel

The magnetic induction $B$, magnetic field strength $H$ and magnetisation $M$ in a material are related by the general constitutive equation

$$B = \mu_0(H + M).\tag{8}$$

For ferromagnetic steels including D6ac, the relationship between $B$ and $H$ depends on the prior magnetic history of the specimen and is described using an initial $B$-$H$ curve ('normal curve') and a series of hysteresis loops. The magnetic properties of D6ac steel of the same stock as that used in the F–111 fleet and having the same heat treatment were measured experimentally and are published in a previous report [8]. The main features are presented in Table 1 and summarised below. We adopt the CGS system of units (Gauss and Oersted) for $B$ and $H$, to maintain consistency with RAAF specifications for MRT inspection procedures.*

The variation of $B$ with applied magnetic field strength $H$ for an initially demagnetised D6ac test specimen is shown in Figure 3. The relative magnetic permeability

$$\mu_r = B/(\mu_0 H)\tag{9}$$

and differential relative magnetic permeability

$$\mu_r' = \frac{1}{\mu_0}\frac{dB}{dH}\tag{10}$$

are shown as a function of $H$ in Figure 4. The differential permeability data were obtained by numerical differentiation of the $\mu_r$ data in Figure 4.

Table 1.    Magnetic properties of D6ac steel

|  | SI units | CGS Units |
| --- | --- | --- |
| Coercive force $H_c$ | 2010 A/m | 25.2 Oe |
| Remanent flux density $B_r$ | 1.28 T | 12.8 kG |
| Initial relative permeability $\mu_i$ | $77 \pm 2$ | $77 \pm 2$ |
| Maximum relative permeability $\mu_{max}$ | $\mu_{max}$ =350 at 2700 A/m | $\mu_{max}$ =350 at 34 Oe |
| Maximum differential relative permeability $\mu'_{max}$ | $\mu'_{max}$ =650 at 2150 A/m | $\mu'_{max}$ =650 at 27 Oe |

---

* The conversion from CGS electromagnetic units to the corresponding SI units (Tesla and A/m) is as follows: 1 Oersted (Oe) = 79.58 A/m and 1 Gauss (G) = 0.1 mT.
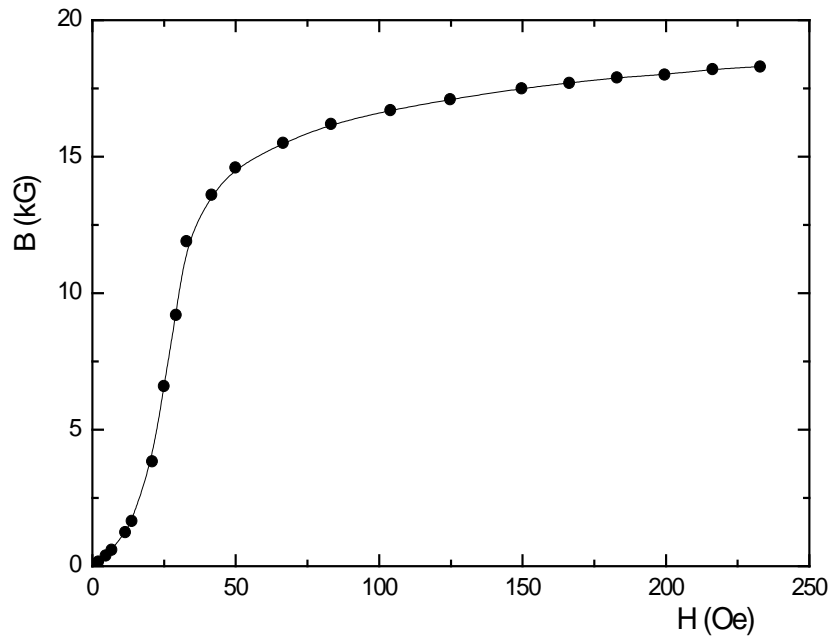
DSTO-TR-3032



*Figure 3.   Normal magnetic induction curve for D6ac steel (CGS units)*
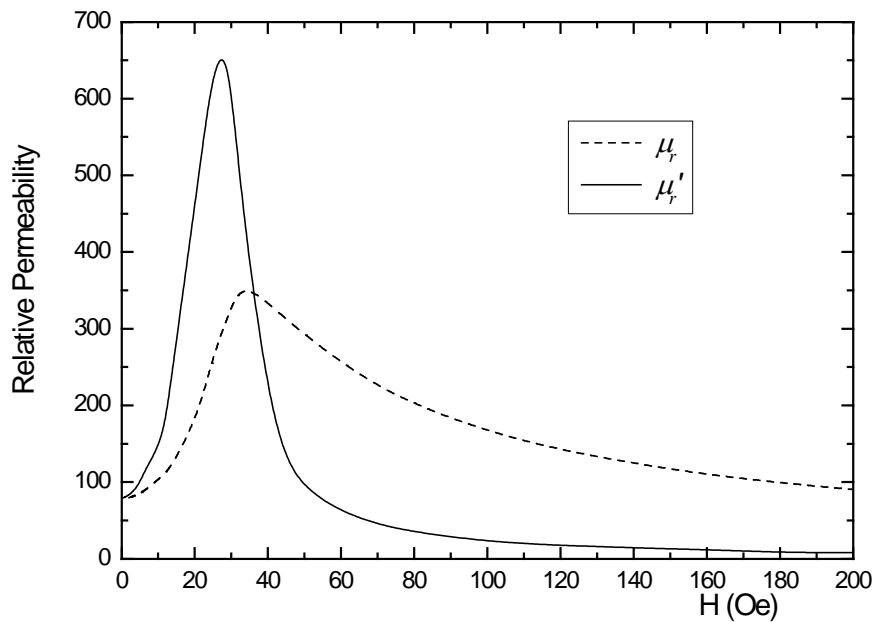


*Figure 4.   Relative magnetic permeability (dashed) and differential relative magnetic permeability (solid) for D6ac as a function of magnetic field strength (CGS units)*

The major hysteresis curve (or *B–H* loop) for D6ac is presented in Figure 5 and shows the locations on the curve corresponding to the coercive field $H_c$ and magnetic remanence $B_r$. Figure 6 shows a series of minor hysteresis loops obtained by cycling an initially demagnetised specimen between magnetic field strengths $H_{max}$ and $-H_{max}$. The loops correspond to values of $H_{max}$ of 20.1 Oe, 30.1 Oe, 46.5 Oe and, for the major loop, 251 Oe.
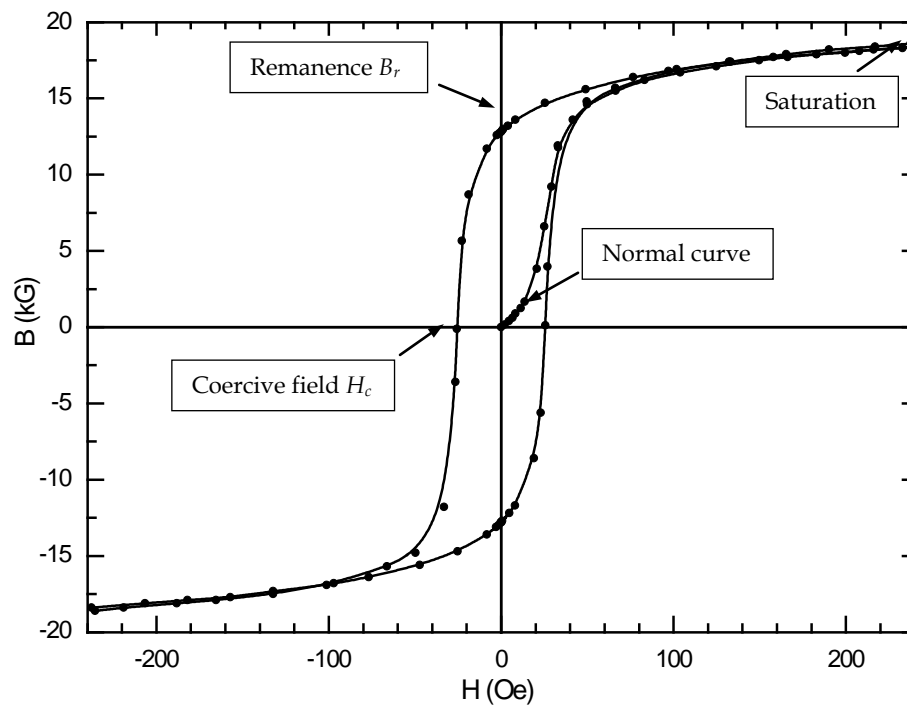
*Figure 5.  Magnetic hysteresis curve for D6ac (CGS units). The normal curve is also shown for comparison.*
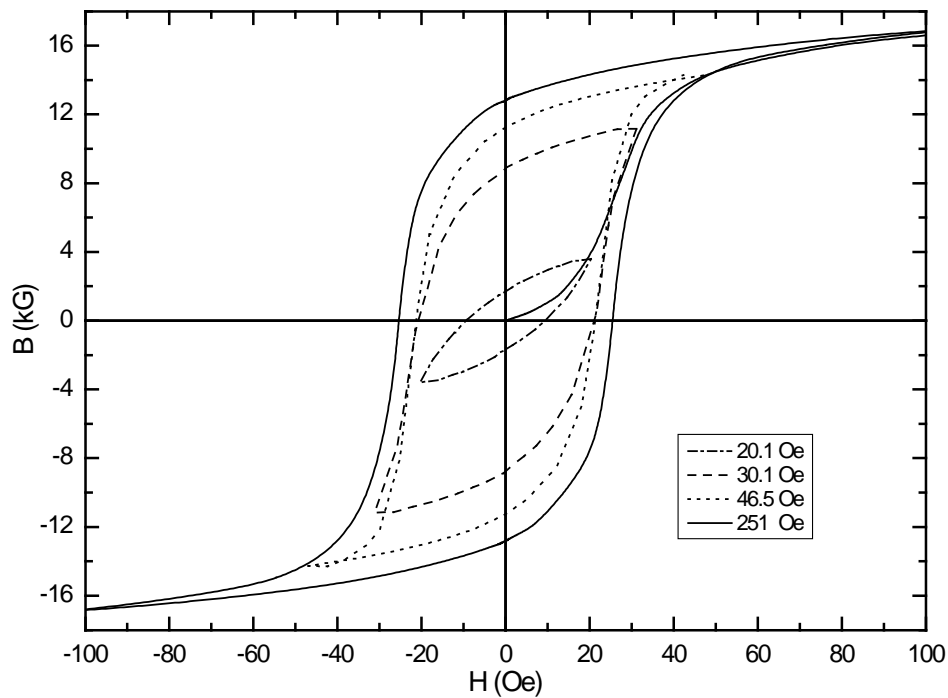


*Figure 6.  Minor hysteresis loops for D6ac (CGS units). The maximum excursion $H_{max}$ for each loop is indicated. Note the difference in scale compared with Figure 5.*

In air, the magnetisation is negligible ($M = 0$) and hence from Eq. (8) the magnetic flux density $B$ in air is proportional to the magnetic field strength $H$:

$$B = \mu_0 H \, . \tag{11}$$

Thus, in the CGS system of units for which $\mu_0 = 1$, a magnetic field strength $H = 1$ Oe measured in air corresponds to a magnetic flux density in air ($B$) of 1 G.[*] Within the material, the relationship between $B$ and $H$ is a complicated function of the magnetic history of the specimen as illustrated by the minor hysteresis loops in Figure 6.

## 2.4  Fields at the air-steel interface

The fundamental relationships between the magnetic fields at the surface of a magnetic material such as D6ac steel are depicted in Figure 7, where the normal component of **B** and the tangential component of **H** are mathematically continuous across the air-steel interface. The significance of the latter boundary condition for practical MRT cannot be underestimated. It states that the tangential field strength measured immediately above the surface of the magnetic material is equal to the tangential magnetic field just below the surface of the specimen,

$$H_t(air) = H_t(steel) \, . \tag{12}$$

Thus, gaussmeter measurements of the tangential component of magnetic field strength in air immediately above the surface of a D6ac component can be used as an approximate measurement[†] of the tangential component of magnetic field strength within the material immediately below the surface. Furthermore, if (and only if) the magnetic history of the specimen is known, the state of internal magnetisation of the component can be inferred using the known magnetic properties of D6ac, as discussed in detail below.
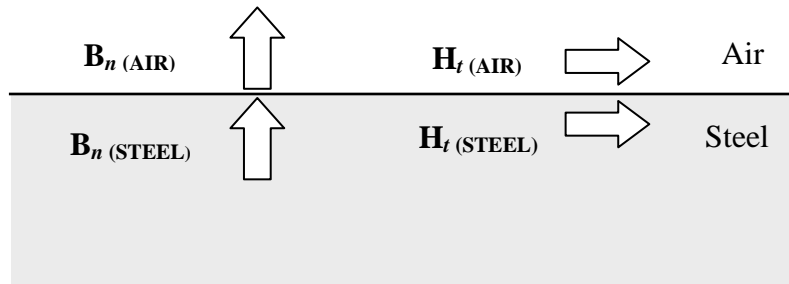


*Figure 7.  Boundary conditions at the surface of the test specimen. The component of **B** normal to the surface and the component of **H** tangential to the surface are mathematically continuous across the steel-air boundary.*

---

[*]Instruments used for the measurement of magnetic flux density typically display readings in Gauss. The corresponding magnetic field strength in Oe is the simply the same numerical value.

[†] 'Approximate' because it is impractical with current instrumentation to measure in air exactly at the surface but only at some finite distance above it.

Consider the case relevant to active-field MRT for which the magnetisation of the D6ac steel will lie on the normal induction curve[*] (Figure 3). If, for example, a tangential field of $H_t$ = 50 Oe[†] is measured at the surface of the specimen, the field within the specimen is also $H_t$ = 50 Oe, and from Figure 3, $B_t$ = 14 kG just inside the steel. Furthermore, from Figure 4, the magnetic permeability at $H_t$ = 50 Oe is approximately 300.

Next, as described in the companion report [11], consider the case relevant to residual-field MRT for which the $B$–$H$ characteristics of the specimen are located in the second quadrant, given in Figure 8. If, for example, a tangential field of $H_t$ = -20 Oe[‡] were to be measured on the surface of the specimen, then the tangential field within the specimen would also be $H_t$ = -20 Oe. However, as shown in Figure 8, without knowledge of the prior magnetic history of the specimen (in this case the maximum value of the initially applied field $H_{max}$), it is not possible to determine which of the curves is applicable and it would be possible for $B_t$ to lie anywhere between 0 and 7.5 kG.

Hence, knowledge of the prior magnetic history of the test specimen is critically important in residual-field MRT. Without it, the specimen magnetisation cannot be uniquely determined.
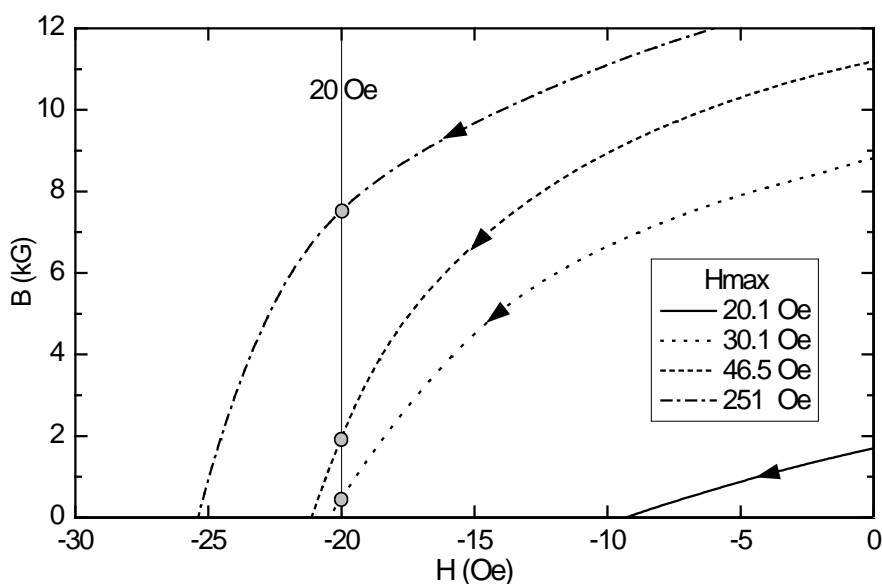


*Figure 8.  Enlarged view of the series of B-H curves for D6ac steel corresponding to different values of $H_{max}$ (CGS units). Each curve corresponds to the 2nd quadrant of the minor hysteresis loops shown in Figure 6. B inside the specimen is not uniquely determined by H alone (in this example 20 Oe) but can take different values ranging from 0 to 7.5 kG, depending on the prior magnetic history of the specimen.*

[*] It is standard practice in active-field MRT to start the inspection with the specimen in a demagnetised condition.

[†] In air, $H_t$ = 50 Oe corresponds to a magnetic flux density $B_t$ = 50 G, which would be the numerical value registered by a gaussmeter.

[‡] Again, in air $H_t$ = 20 Oe corresponds to a magnetic flux density $B_t$ = 20 G.

# 3. Magnetic Field Strength Requirements for Active-Field Magnetic Rubber Testing of D6ac

*In summary, although code and specification requirements are very detailed, the practice of determining if sufficient flux is being generated is not an exact science. The ideal way to determine if sufficient flux is generated in the part is to have an identical part with an actual discontinuity of the size, shape and type as those being sought. If these can be reliably found, then the probability of finding an identical or larger discontinuity in the test part is very high.* – C J Hellier [44]

For active-field MRT, the magnetic field is specified in terms of the applied field strength and orientation, and the duration of time for which the field to be is applied during curing. Adequate magnetisation is ensured by specifying the field strength through measurements of the tangential component of $H$ on the surface of the specimen in the region of interest using a Hall-effect or gaussmeter probe[*]. The required field value will depend on the magnetic properties of the steel involved as well as the magnetic rubber formulation. For example, higher fields are required for crack detection if the coercive field of the grade of steel is increased [45]. Field values quoted in the general MRT literature[†] are of limited value in confirming the requirements for inspection of a specific UHS steel such as D6ac, because the published data contains insufficient information on either the type of steel, or the magnetic rubber formulation, or both [3, 4, 12, 46, 47].

The values recommended by the RAAF Nondestructive Testing and Composite Technology (NDT&CT) for general active-field MRT of D6ac steel are given in Table 2. For these active-field inspections, the field is applied using either permanent magnets or continuous DC electromagnets but not pulsed DC or AC field sources.

*Table 2.    Recommended magnetic fields for ad-hoc MRT of D6ac components [48]. The values refer to the tangential component of magnetic flux density measured immediately above the region of interest using a Hall-effect or gaussmeter probe.*

| Test Area | Magnetising Method | Magnitude and Duration |
|---|---|---|
| Bare holes, corners | Permanent magnet | 25–30 G for duration of pot life |
| Bare holes, corners | Electromagnet | 25–30 G for 90s continuous |
| Bare blended, surfaces | Permanent magnet | 25–30 G for duration of pot life |
| Bare blended, surfaces | Electromagnet | 25–30 G for 90s continuous |

---

[*] Limitations on the application of gaussmeters for the measurement of magnetic fields in MRT are given in another publication by one of the authors [8].

[†] There is very little detailed published literature on MRT. The 1978 MRT Patent [4] gives a recommended magnetic field for uncoated metal of 150 G and duration of 1 minute, but neither the recommended MRT formulation, nor types of steel are specified.

According to the literature for magnetic test methods, the maximum sensitivity for detection of surface-breaking defects using active-field MPI occurs for values of $H$ in the vicinity of the inflection point (or 'knee') of the $B$–$H$ curve [15], or, equivalently, in the vicinity of the peak in the differential magnetic permeability [16, 49, 50]. This optimum value is rather broadly defined: the field must be sufficiently high to give adequate sensitivity but not so high as to produce a large number of false indications. A dissenting view (more relevant to magnetically soft steels) is put by Oehl and Swartzendruber [51] who conclude that the optimum applied field is larger than that corresponding to the maximum permeability and is simply the largest field practically available without producing unwanted background signals.

For D6ac, the inflection point in the normal curve data (Figure 3) or the peak in the differential permeability (Figure 4) occurs for a magnetic field strength of ~ 27 Oe, corresponding to a tangential component of $B$ measured at the surface of the test specimen of ~ 27 G. This value is consistent with the advisory levels used by the ADF, where a value in the range 25–30 Oe is recommended for active-field inspections of bare surfaces using a permanent magnet (Table 2).

An alternative criterion is given in British Standard BS EN ISO 9934-1:2001 for magnetic particle inspection [52], which specifies that the minimum magnetic field strength $H$ shall correspond to a flux density $B = 10$ kG within the material. From the normal induction curve for D6ac shown in Figure 3, a flux density of 10 kG corresponds to a magnetic field strength $H = 30$ Oe or $B = 30$ G. Although at the upper limit of the range in Table 2, this value is consistent with Table 2, considering the subtle differences between MRT and MPI.

The most robust support for magnetic field strength requirements for active-field MRT of D6ac steel is provided by a previous DSTO experimental probability of detection (POD) trial [5, 6]. From this POD trial it was demonstrated that a tangential field of 25–30 Oe was sufficient to achieve a value for the smallest crack that can be reliably detected, $a_{NDI} = 0.3$ mm (0.012 inch)[*] for a component having a good surface finish. The background to the DSTO POD trial is described below.

In the DSTO POD trial, a set of test specimens containing known laboratory-grown cracks were inspected using active-field MRT with a tangential magnetic field strength of 25–30 Oe. The test specimens contained elongated holes representative of the geometry of the Fuel Flow Vent Holes ('mouse holes') within the wing pivot fitting of the F–111 aircraft. Fatigue cracks were grown under fatigue spectrum loading at the radius runout location within the holes. The inspections were performed by six RAAF NDT technicians with different levels of experience in MRT. The test coupons were mounted inside an F-111 wing-pivot fitting to simulate the access conditions encountered in practice. Approximately equal numbers of cracked and uncracked specimens were inspected.

---

[*] Imperial units (inch) as well as SI units (mm) will be used for $a_{NDI}$ and crack dimensions in the remainder of this report to be consistent with the conventions then current for F-111 aircraft. 1 inch = 25.4 mm.

The results of this previous DSTO POD trial are reproduced in Figure 9. The input data used in the analysis are the results of the field inspections in the form of ordered pairs (defect size, hit/miss) where the defect size is the surface length of the crack inspected and the hit/miss parameter is the inspection result (a hit = 1 or a miss = 0 for that particular inspection). To produce the POD curve shown in Figure 9, maximum likelihood estimation (MLE) is used to fit a log-normal cumulative distribution function to the hit/miss POD data as a function of defect size.  A lower 95% confidence limit is then placed on the POD curve to account for statistical uncertainty in the POD estimate due to the finite size of the inspection data set ($N = 140$). According to this approach, $a_{NDI}$ is identified with $a_{90/95}$, the defect size for which a POD of 90% has been demonstrated with 95% statistical confidence, which equates to reading the 90% POD crack size off the lower 95% lower confidence limit curve. According to Figure 9, $a_{NDI} = a_{90/95} = 0.289$ mm (0.0114 inch), which becomes 0.3 mm (0.012 inch) when conservatively rounded upwards.

It is likely that reducing the applied field strength below the range 25–30 Oe will decrease the POD for small cracks, such that only successively larger cracks can be reliably detected as the field is reduced. Ultimately, if the field is reduced too greatly, the technique will become completely ineffective. The results of an experimental program performed in order to investigate the effect of decreasing field strength are presented in Section 4 as part of a wider study into the role of the perpendicular (normal) component of magnetic field at different levels of tangential field strength.  The effect of magnetisation duration for active-field MRT is discussed briefly in Section 5.
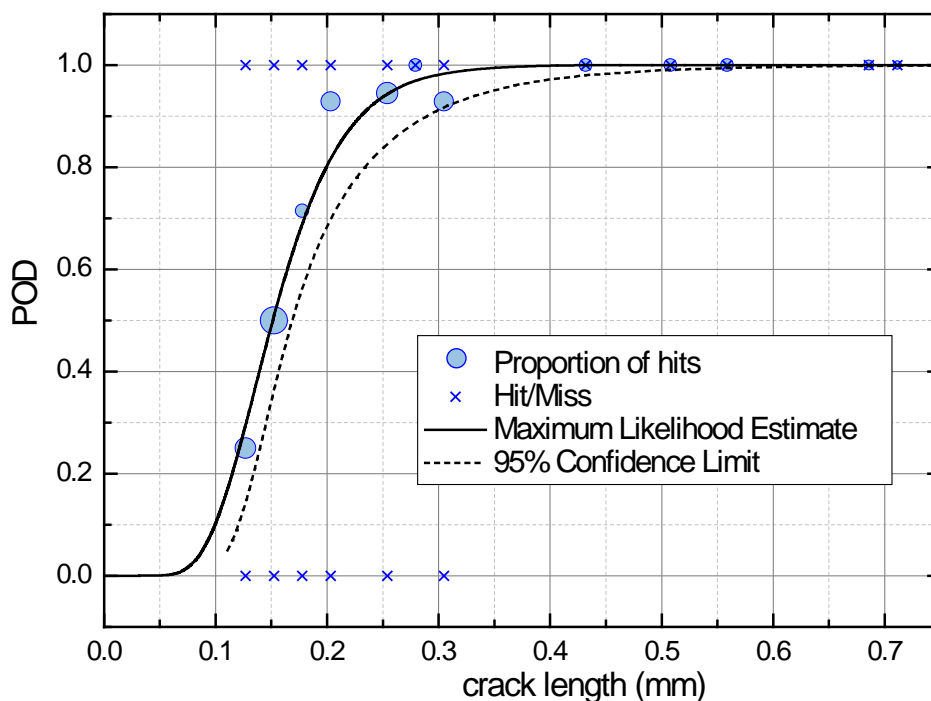


*Figure 9.   Active-field MRT inspections: probability of detection as a function of surface crack length for fatigue cracks in D6ac F-111 mouse hole specimens. Figure adapted from references [5, 6].*

# 4. Effect of Perpendicular Magnetic Fields in Active-Field Magnetic Rubber Testing of D6ac

Ideally, when performing active-field MRT, the magnetic field should be tangential (parallel) to the surface of the component under test and the normal (perpendicular) component of magnetic field in the region of interest should be as small as possible [7, 53]. It has been demonstrated in previous work that the presence of excessive normal fields can cause distortion, weakening, or masking of MRT indications from fatigue cracks [7]. Based on the limited experimental results from these initial trials, it was recommended that the magnitude of the normal component of magnetic field should not exceed the tangential component of magnetic field throughout the test area. These previous trials were limited to two cases where the tangential field[*] was fixed at 25–30 G and either (i) the magnitude of the normal field was negligible (< 5 G) or (ii) the magnitude of the normal field was approximately equal to that of the tangential field.

A further series of experiments was performed to examine the effect of a wider range of tangential and normal magnetic field strengths on crack detectability. The results are presented below.

## 4.1 Normal-tangential field matrix trial: experiment

The experimental measurements were performed using six of the D6ac mouse hole geometry test coupons fabricated for the earlier MRT POD study conducted jointly by DSTO and RAAF NDT&CT [5, 6]. The specimens contained eleven well-characterised fatigue cracks with crack lengths of up to 2.3 mm (0.090 inch). The crack geometry and surface lengths are given in Appendix A. The MRT test procedure used is given in Appendix B. The inspections were performed by experienced Level II nondestructive inspectors under contract to DSTO.

MRT casts were obtained for each of the coupons using the test matrix of tangential and normal fields defined in Table 3.The matrix comprised three levels of tangential field:

- 27 ± 1 G, the midpoint of the preferred range 25–30 G,

- 20 ± 1 G, the minimum of the mid range 20–25 G,

- 16 ± 1 G, the minimum allowable field for any ADF MRT procedure,

combined with four different levels of normal field. The normal fields were selected to give a ratio of normal to tangential magnetic flux density measured in air ($B_n : B_t$) of 0:1[†], 1:1, 2:1, 3:1 and 4:1 (only for 16 G tangential).

---

[*] For convenience, the magnetic field strength and the magnetic flux density (when both measured in air) are referred to simply as the "field" in this section.

[†] The ratio "0:1" indicates that the normal field was negligible (< 5 G).

*Table 3.*   *Test Matrix. Specification of tangential ($B_t$) and normal components ($B_n$) of magnetic flux density for MRT trials*

| Tangential Flux Density ($B_t$) | Normal-to-tangential-field ratio $B_n : B_t$ | | | | |
|---|---|---|---|---|---|
| | 0:1 | 1:1 | 2:1 | 3:1 | 4:1 |
| 27 ± 1 G | $B_n < 5$ G | $B_n = 27 \pm 3$ G | $B_n = 55 \pm 5$ G | $B_n = 80 \pm 8$ G | – |
| 20 ± 1 G | $B_n < 5$ G | $B_n = 20 \pm 2$ G | $B_n = 40 \pm 4$ G | $B_n = 60 \pm 6$ G | – |
| 16 ± 1 G | $B_n < 5$ G | $B_n = 16 \pm 2$ G | $B_n = 32 \pm 3$ G | $B_n = 48 \pm 5$ G | $B_n = 64 \pm 5$ G |

The field was applied via a 'powershoe' magnet assembly made up from an Alnico permanent magnet, steel pole pieces and field-adjusting shims. The required tangential and normal magnetic fields were obtained by adjusting the dampening shims and by rotating the position of the magnet assembly, as shown in Figures B3–7 of Appendix B. It was possible to achieve a field ratio $B_n : B_t = 4{:}1$ for a tangential field of 16 G but not at the higher tangential field strengths. Accurate and repeatable measurements of $B_t$ and $B_n$ in the test region were ensured by using a precisely machined Hall-probe guide which was inserted into the mouse hole during the measurements [7].

Once the MRT inspections had been performed, each silicone rubber cast was examined using an optical microscope and the crack indications were photographed at low magnification (ranging from 6× to 25×). The lengths of the crack indications in the bore of the mouse hole were measured and qualitative descriptions of the strength of the indications were recorded.

## 4.2  Normal-tangential field matrix trial: results and analysis

The length and strength of the crack indications are tabulated in Appendix A for the matrix of applied field conditions. The results showed a general trend for the strength of the indication, and hence the crack detectability, to decrease: (i) when the strength of tangential field was reduced from 27 to 20 G and from 20 to 16 G, and (ii) when the normal-to-tangential field ratio was increased.

An empirical method was used to quantify this reduction in inspection reliability with magnetic field conditions. The method was based on the assignment of a notional POD to each recorded crack indication using a scale from 0 to 1 in increments of 0.1, based on a collective assessment of the appearance and strength of the crack indications made by a group of DSTO NDE researchers with experience in MRT inspections. The notional POD assignments for each crack indication are also given in Appendix A. A POD analysis was then employed in order to estimate values of $a_{90}$ for each of the field conditions for the assigned notional POD values. In view of the small sample size, the semi-quantitative nature of the POD assessment, and the absence of defined confidence limits on the POD

estimates[*], a safety factor of 1.5 was then applied to the estimated value of $a_{90}$ to obtain an estimate of $a_{NDI}$. The variation of the estimated $a_{NDI}$ with field conditions for this trial is plotted as solid symbols in Figure 10.

The suggested values for the corresponding design limits for active-field MRT are given in Table 4. These values are not a simple transcription of the estimated $a_{NDI}$ data points presented in Figure 10, but after review, were rounded up or down to an appropriate multiple of 0.005 inch to reflect the uncertainty of these values compared with those obtained from the previous large-scale POD trial [5, 7]. The use of normal-to-tangential-field ratios greater than 3:1 is not recommended, so the results obtained at a tangential field of 16 G for a normal to tangent field ratio of 4:1 are not included in Table 4.

A limited trial with tangential fields in the range 10–16 G with a field ratio of 2:1 was also undertaken, giving an estimated $a_{NDI}$ = 1.4 mm (0.055 inch). The use of tangential fields below 16 G is also not recommended nor used for ADF MRT inspections.
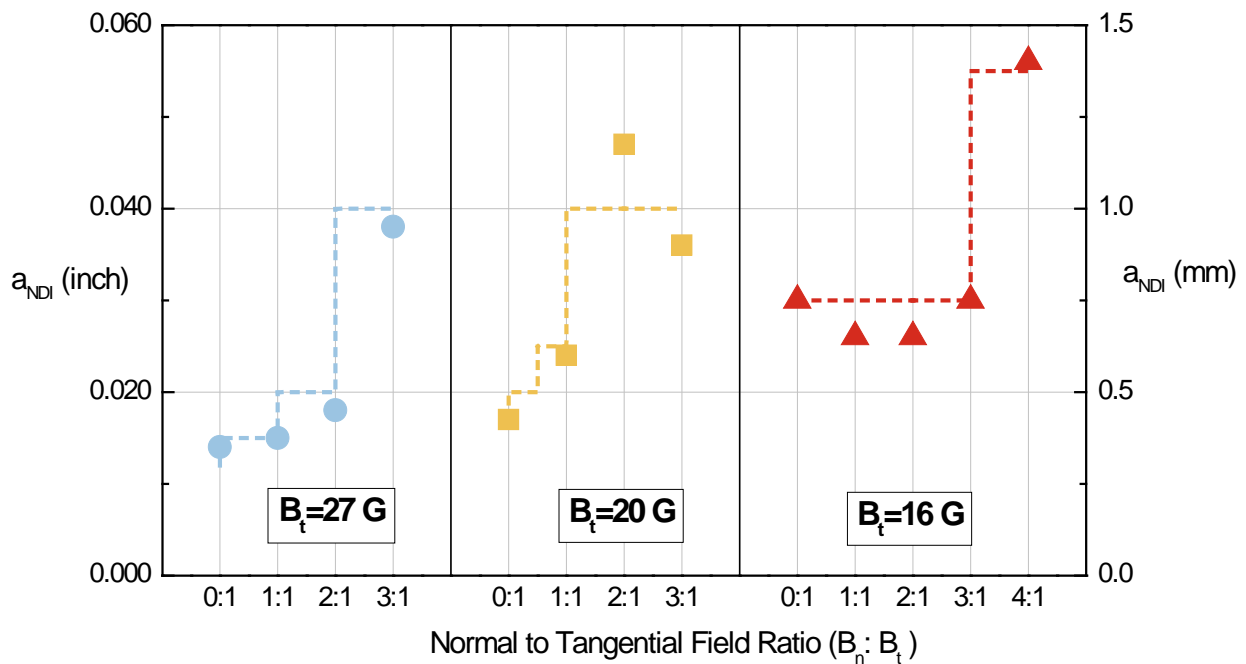


Figure 10. *Matrix trial. Estimated values of $a_{NDI}$ for active-field MRT at tangential fields of 27 G, 20 G and 16 G for a range of normal-to-tangential field ratios ($B_n : B_t$). The symbols denote $a_{NDI}$ based on $1.5 \times a_{90}$ determined from the data in Appendix A. The dashed lines denote the suggested design limits for $a_{NDI}$ based on these data, given in Table 4.*

---

[*] By convention, $a_{NDI}$ values are normally based on the defect size for which 90% POD has been demonstrated with a 95% statistical confidence level through empirical tests. However, the nature of the available data do not allow computation of confidence levels, requiring the alternate approach used here of applying a safety factor of 1.5 to $a_{90}$.

*Table 4.* *Indicative values of $a_{NDI}$ for tangential and normal field combinations in active-field MRT of D6ac of highly polished uncoated surfaces using permanent magnets. (Not applicable to residual-field or central conductor inspections)*

| Tangential Field $(B_t)$ | Normal-to-tangential-field ratio $(B_n : B_t)$ | | | | |
|---|---|---|---|---|---|
| | ≤ 0.5:1 | ≤ 1:1 | ≤ 2:1 | ≤ 3:1 | >3:1 |
| 25-30 G | 0.38 mm 0.015 inch[a] | 0.38 mm 0.015 inch | 0.5 mm 0.020 inch | 1.0 mm 0.040 inch | Not permitted |
| 20-25 G | 0.5 mm 0.020 inch[b] | 0.63 mm 0.025 inch | 1.0 mm 0.040 inch | 1.0 mm 0.040 inch | |
| 16-20 G | 0.76 mm 0.030 inch | 0.76 mm 0.030 inch | 0.76 mm 0.030 inch | 0.76 mm 0.030 inch | |

(a) Value is taken to be the same as for < 1:1 normal-to-tangential-field ratio.
(b) Value linearly interpolated between values determined for 0:1 and 1:1 normal-to-tangential-field ratios at 20 G tangential field strength.

The main features of the estimated $a_{NDI}$ values (plotted as solid symbols in Figure 10) are:

- The highest inspection reliability (smallest $a_{NDI}$) in the test matrix occurs for a tangential field of 27 G combined with a normal field of 5 G or lower. The inspection sensitivity and reliability are degraded when there is a departure from these conditions;

- The inspection reliability decreases ($a_{NDI}$ increases) when the tangential field is reduced;

- The inspection reliability decreases ($a_{NDI}$ increases) with increasing normal field for tangential fields of 27 G and 20 G;

- For the minimum allowable field $B_t = 16$ G, $a_{NDI}$ initially decreases slightly when the normal field is increased. This exception to the general trend is possibly associated with the low initial tangential field strength so that the primary effect of the normal component of field to increase the overall magnitude of the field $|\boldsymbol{B}| = \sqrt{B_t^2 + B_n^2}$ , rather than through a change in field direction.

## 4.3 Normal-tangential field matrix trial: discussion

According to Table 4, the highest inspection sensitivity and reliability (smallest $a_{NDI}$) are achieved when the tangential field is in the range 25–30 G and the ratio of the normal to tangential field components is 1:1 or less. The inspection reliability decreases once the field conditions depart from these optimum conditions, confirming the predictions of a previous, more limited study [7].

The minimum value of $a_{NDI} = 0.38$ mm (0.015 inch) given in the first cell of Table 4 is larger than the $a_{90/95}$ value of 0.30 mm (0.012 inch) obtained from the previous DSTO/RAAF POD trial for active-field MRT. In this previous trial, described briefly in Section 3, the

tangential magnetic field strength was in the range 25 – 27 G with a nominally zero value of normal-tangential field ratio [5]. Table 4 takes the values of $a_{NDI}$ at the upper limit of the quoted normal-tangential field ratio of $\leq 0.5 : 1$ and, rather than interpolating between values, a more conservative approach is taken by adopting the $a_{NDI}$ value for the 1:1 normal-tangential field ratio.

The results in Table 4 are indicative of the performance of active-field MRT of D6ac for uncoated, highly polished surfaces using permanent magnets and are not necessarily applicable to other broader inspection conditions (for example, to cases of poor surface condition, or for central conductor inspections and other configurations or magnetisation methods).

The presence of a normal magnetic field component leads to a general drift of magnetic particles from one side of the crack to the other, leading to the distinctive asymmetrical 'white banding' seen in MRT casts that have been set in the presence of a significant normal field component, Figure 11. These bands on one or the other side of the black crack indication appear white because they contain a very low density of magnetic particles so that the underlying white pigment of the base rubber becomes more apparent. The location of the white band swaps from one side of the crack to the other when the normal field is reversed in sign. The results of theoretical calculations modelling the effects of a normal magnetic field in active-field MRT are given in Section 4.4.

The recommendation in Table 4, that normal to tangential field ratios greater than 3:1 should not be used in active-field MRT, is consistent with the recommendations made by Shelikhov [53] for the related magnetic technique of MPI.

It is not understood why the inspection reliability appears to increase slightly when the tangential field is reduced from 20 G to 16 G for the field ratios 2:1 and 3:1. The significance of this result might become clearer from the results of a large scale POD trial. However, in the authors' opinion, there would be limited value in further exploring a regime which is far from the optimum conditions required for reliable MRT inspection.
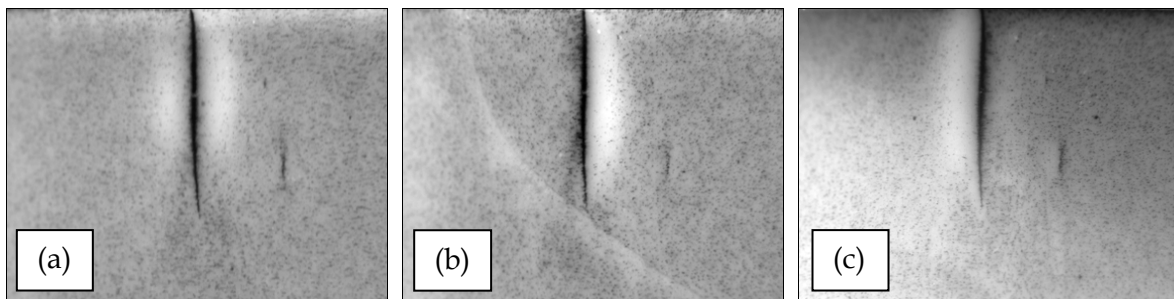


*Figure 11. MRT casts of cracks showing the effect of a normal component of magnetic field. In all cases $H_t \sim 27\ Oe$ but $H_n$ varies: (a) 6 Oe – a low value, (b) 27 Oe – equivalent normal and tangential field amplitudes, and (c) -27 Oe – normal field reversed in direction. The location of the white band is reversed when the normal field is reversed. The larger crack is 2.3 mm (0.090 inch) long and the smaller crack is 0.30 mm (0.012 inch) long. Reproduced from previous work by the same authors [7].*

## 4.4  Two-dimensional numerical calculations: effect of the normal field

A simplified 2-D theory was developed to examine the effect of a normal component of field in order to improve the fundamental understanding of the active-field MRT experiments described above.

The magnetic fields in the vicinity of a 2-D crack are shown schematically in Figure 12 and consist of the leakage field due to the crack $H_{crack}$, together with the local tangential ($H_t$) and normal ($H_n$) components arising from the remote applied field and the magnetisation of the specimen. According to this construct,

$$\boldsymbol{H} = \hat{\boldsymbol{y}}\, H_n + \hat{\boldsymbol{x}}\, H_t + \boldsymbol{H}_{crack}. \tag{13}$$

Substituting Eq. (13) into Eq. (2), the magnetic force on a particle is given by

$$\boldsymbol{F}_{mag} = \mu_0 V \,\nabla\left[\left(H_t + H_{crack}^x\right)^2 + \left(H_n + H_{crack}^y\right)^2\right], \tag{14}$$

where $H_{crack}^x$ and $H_{crack}^y$ denote the $x$ and $y$ components of the leakage field from the crack.

Assuming that $H_t$ and $H_n$ are uniform in the region of the crack, the individual $x$ and $y$ components of the magnetic force in Eq. (14) can be written in the form

$$F_{mag}^x = 2\mu_0 V\left[\left(H_t + H_{crack}^x\right)\frac{\partial H_{crack}^x}{\partial x} + \left(H_n + H_{crack}^y\right)\frac{\partial H_{crack}^y}{\partial x}\right],$$
$$F_{mag}^y = 2\mu_0 V\left[\left(H_t + H_{crack}^x\right)\frac{\partial H_{crack}^x}{\partial y} + \left(H_n + H_{crack}^y\right)\frac{\partial H_{crack}^y}{\partial y}\right]. \tag{15}$$
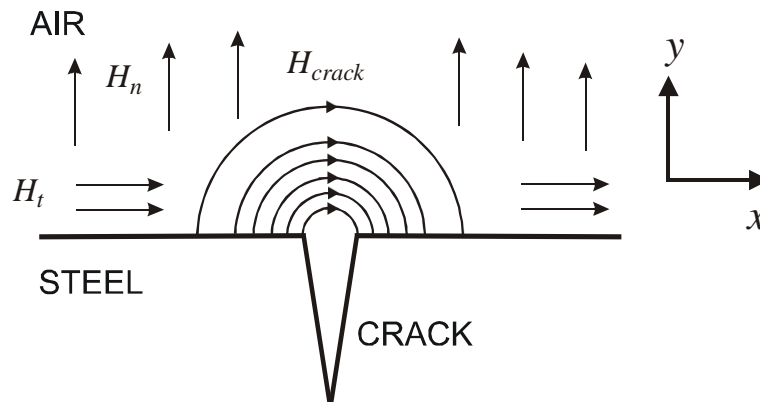


Figure 12. Schematic showing the behaviour of magnetic fields in the vicinity of a 2-D crack, in particular the leakage field due to the crack ($H_{crack}$), and the normal ($H_n$) and tangential ($H_t$) components due to the remote applied field and specimen magnetisation

The significance of Eq. (15) becomes clear once the individual contributions to the magnetic force $F_{mag}$ are isolated, so that

$$F_{mag}^x = F_0^x + F_n^x, \ F_{mag}^y = F_0^y + F_n^y, \tag{16}$$

where $F_0$ is the usual magnetic force due to the crack in the absence of a normal field component,

$$F_0^x = 2\mu_0 V \left[ \left( H_t + H_{crack}^x \right) \frac{\partial H_{crack}^x}{\partial x} + H_{crack}^y \frac{\partial H_{crack}^y}{\partial x} \right],$$

$$F_0^y = 2\mu_0 V \left[ \left( H_t + H_{crack}^x \right) \frac{\partial H_{crack}^y}{\partial x} - H_{crack}^y \frac{\partial H_{crack}^x}{\partial x} \right], \tag{17}$$

and $F_n$ is the additional force on the particle due to the normal component of field,

$$F_n^x = 2\mu_0 V H_n \frac{\partial H_{crack}^y}{\partial x},$$

$$F_n^y = -2\mu_0 V H_n \frac{\partial H_{crack}^x}{\partial x}. \tag{18}$$

The Cauchy identities relating the derivatives of the magnetic field [21]

$$\frac{\partial H_{crack}^x}{\partial y} = \frac{\partial H_{crack}^y}{\partial x}, \quad \frac{\partial H_{crack}^y}{\partial y} = -\frac{\partial H_{crack}^x}{\partial x}, \tag{19}$$

have been used in the derivation of Eqs (17) and (18).

Some general observations that can be made from Eq. (18) concerning the additional force $F_n$ due to a normal component of field:

- From the symmetry of the leakage field shown in Figure 12, the effect of the force $F_n$ is to preferentially transport particles away from one side of the crack and to deposit particles on the other side of the crack, leading to a distinctive white band on one side of the crack and a darker band on the other side (Figure 11).

- If $H_n$ is reversed the force $F_n$ is reversed. It follows that the related contrast of a MRT crack indication will be reversed about the line of the crack if the normal field is reversed. This is consistent with the experimental observations (Figure 11) [7].

The forces on a magnetic particle introduced by the normal component of magnetic field are shown in Figure 13 . In these calculations, the force is calculated using Eq. (16) with the crack leakage field assumed to take the form used by [21, 24, 42],

$$H^{x}_{crack} = \frac{\sigma_s}{2\pi}\left(\arctan\left[\frac{b(x+a)}{(x+a)^2+y(y+b)}\right]-\arctan\left[\frac{b(x-a)}{(x-a)^2+y(y+b)}\right]\right),$$

$$H^{y}_{crack} = \frac{\sigma_s}{4\pi}\log\left[\left(\frac{(x+a)^2+(y+b)^2}{(x-a)^2+(y+b)^2}\right)\left(\frac{(x-a)^2+y^2}{(x+a)^2+y^2}\right)\right],$$

(20)

where $b$ is the crack depth, $2a$ is the crack opening width and $\sigma_s$ is the magnetic pole density

$$\sigma_s = \frac{H_{0t}\,\pi(\mu_r-1)\,n}{(n+\mu_r)\arctan(n)}.$$

(21)

In Eq. (21), $n = b/a$ is the aspect ratio of the crack, $\mu_r$ is the relative magnetic permeability of the specimen and $H_{0t} = H_t$ is the tangential component of the remote applied magnetic field strength. As shown in Figure 12, the boundary between the specimen and air is at $y = 0$ and the mouth of the crack is located at $x = 0$.

The following parameters were used in performing the calculations resulting in Figure 13: $b = 0.25$ mm, $a = 5$ μm, $\mu_r = 200$ and $H_{0t} = 25$ Oe, which are typical values found in the practical application of active-field MRT to the detection of cracks in D6ac steel. Forces were calculated in the case of (a) zero normal field and (b) a normal field of 50 Oe, with in both cases the tangential field $H_{0t} = 25$ Oe. The results confirm that the effect of a normal component of magnetic field is to preferentially force particles away from one side of the crack and to deposit particles on the other side of the crack, thereby displacing the dark crack indication to one side of the crack mouth and producing a white band on the other.
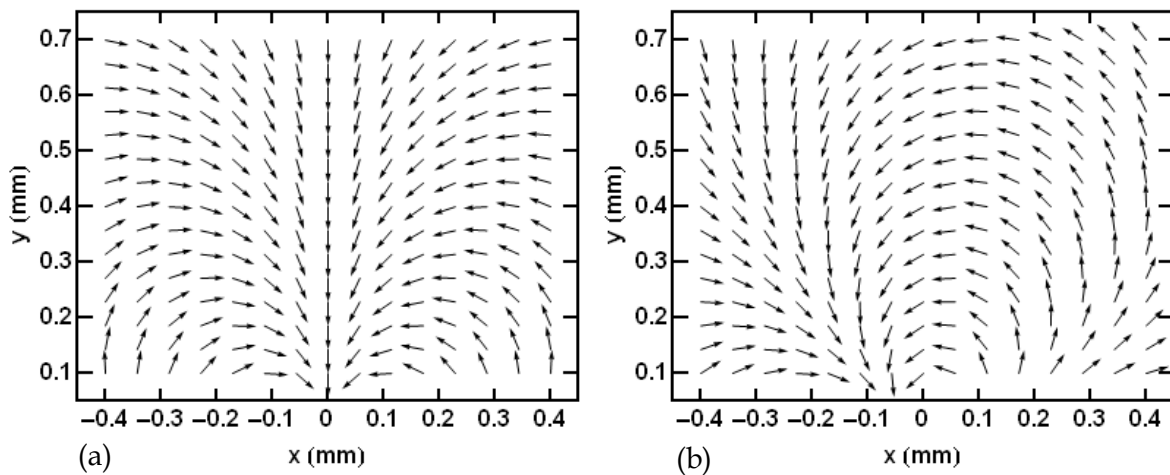


*Figure 13. Effect of a normal component of magnetic field on the magnetic force acting on a particle above a 2-D crack. (a) $H_t = 25$ Oe, $H_n = 0$, (b) $H_t = 25$ Oe, $H_n = 50$ Oe. The forces are calculated from Eqs (16)–(18), assuming a leakage field from the crack of the form given by Eq. (20). The crack mouth is located at (0, 0), and the length of the arrows is related to the magnitude of the force using a logarithmic scale.*

A series of illustrative 2-D computer simulations was also performed to explore the effect of the normal component of magnetic field in more detail. In these simulations, the trajectories of magnetic particles in the vicinity of a crack were calculated by solving the coupled equations of motion, to generate simulated MRT indications due to an infinitely long crack with constant depth [41, 42, 54]. A simple model was used in which gravity and viscosity were neglected and the leakage field due to the crack was described using the form derived by Bowler and Bowler [28],

$$
\begin{aligned}
H_{crack}^{x} &= \frac{2\lambda b}{\pi} \frac{y}{x^2 + y^2} \\
H_{crack}^{y} &= -\frac{2\lambda b}{\pi} \frac{x}{x^2 + y^2}
\end{aligned}
\tag{22}
$$

where $\lambda$ is a scaling factor dependent on the applied field strength and magnetisation, and $b$ is the crack depth.

The simulations were performed using a $65 \times 32$ array of particles distributed quasi-randomly on a grid with dimensions 16 mm ($x$-direction) $\times$ 8 mm ($y$-direction). The particles were each given a random initial velocity to introduce a level of scatter in the appearance of the indications. The magnetic force acting on the particles was calculated using Eqs (16)–(18) combined with Eq. (22). For the purposes of illustration the field strength is measured in arbitrary units. The particle equations of motion were solved over an arbitrary time interval in *Mathematica®*, following a similar approach to other authors [41, 42, 54].

The simulated MRT indication was generated by recording the final $x$-coordinate ($x_{stop}$) of particles that reached the surface of the metal (actually, a height of $y = 10$ μm above the surface to avoid singularity complications) within the time interval of the simulation. From these data, a 2-D scatter plot of ($x_{stop}, z_{stop}$) was produced, where $z_{stop}$ was a uniformly-distributed random variable introduced to give the results of the 2-D simulation the appearance of an indication arising from an infinitely long crack having constant depth.

The results are shown in Figure 14 for $H_t = 1$ and (a) zero normal field, (b) a positive normal field $H_n = 1$ and (c) a negative normal field $H_n = -1$. The simulated indications show the characteristic white bands associated with the presence of a normal component of magnetic field transporting particles from one side of the crack to the other. No quantitative conclusions should be drawn from these results, owing to the simplifications made in developing this simulation.

Attempts were made to develop a more sophisticated quantitative simulation by using the leakage field proposed by Edwards and Palmer [21], and by incorporating the effects of gravity and viscosity in the simulations. However, the degree of improvement obtained from the initial simulation was disappointing, and a significant amount of future research would be required to construct simulations capable of accurately reproducing the more detailed features of MRT indications.
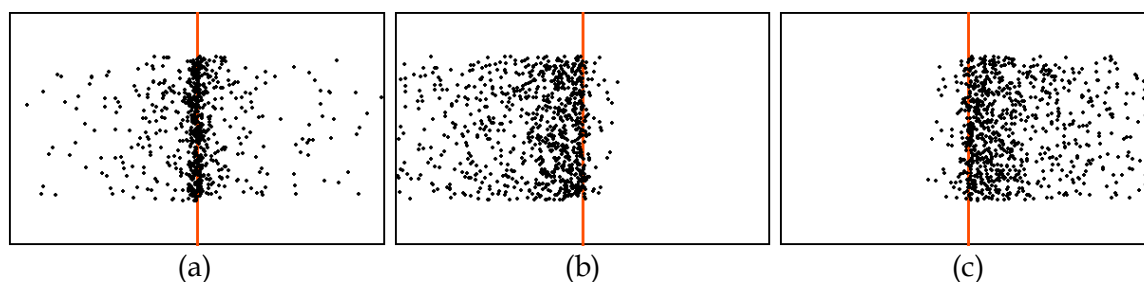
*Figure 14. Effect of a normal field on simulated MRT indications obtained from simple 2-D numerical calculations, employing a magnetic field having arbitrary units. $H_t = 1$ and (a) zero normal field, (b) a positive normal field $H_n = 1$ and (c) a negative normal field $H_n = -1$. The crack location is shown by the vertical orange line.*

# 5. Duration of Magnetisation

The results presented in Section 4 are based on experiments using permanent magnets, for which the duration of magnetisation is at least equal to the pot life[*] of the magnetic rubber mix and of the order of five minutes or greater. A limited series of experimental measurements was performed to investigate the effect of magnetisation duration on MRT crack indications for a range of field strengths. In these tests, the duration of applied magnetisation was 3, 10, 30 or 90 s, with a nominal post-mixing delay of 60 s between mixing the base rubber and catalysts, and transferring the mixed rubber to the mould on the specimen.

The cracks inspected were fatigue cracks of length 2.3, 0.30 and 0.20 mm (0.090, 0.012 and 0.008 inch) present in the bore of the same simulated F-111 mouse hole specimen used in Section 4 and previous POD studies [5]. Measurements were made using these cracks for tangential fields of 29, 22 and 16 G respectively. The magnetic field was produced using a DC electromagnet. The normal component of magnetic field in the region of interest was lower than 6 G.

The trial results were complicated by the unwanted presence of residual magnetisation but clearly demonstrated that distinct MRT crack indications are formed if a tangential magnetic field of 29 G is applied for a period of 90 s. This is consistent with the magnetisation duration of 90 s which is recommended by the RAAF (Table 2). At this level of field, the indications were less distinct when the field was applied for the shorter duration of 30 s and were not evident at all for the shortest durations of 10 s or 3 s.

In these trials, cracks of 0.30 and 0.20 mm (0.012 and 0.008 inch) length were not detected for applied fields of 22 and 16 G respectively for durations of 90 s. This observation is in line with other findings for active-field MRT, for example Table 4 indicates that $a_{NDI} = 0.51$–$0.76$ mm (0.020–0.030 inch) for fields of this level so that there is a reasonable

---

[*] An empirical measure of the time for a given mixture of rubber and catalyst to cure. See section 6.1.

probability that 0.30 and 0.20 mm (0.012 and 0.008 inch) cracks could be missed. For comparison, the recommended field strength for a 'bare blended surface' from Table 2 is 25–30 G.

More comprehensive experimental studies would be required in order to better establish the full effect of magnetisation duration on detection sensitivity.

# 6. Magnetic Rubber Characteristics

The performance of MRT depends not only on the magnetic flux leakage in the vicinity of the crack, but also on the characteristics of the magnetic rubber itself. Preliminary investigations are briefly reported here for two of the more important physical characteristics of magnetic rubber: (i) the variation of magnetic rubber viscosity during cure and the effect on MRT crack indications, and (ii) the size and shape of the magnetic particles in the rubber.

## 6.1 Magnetic rubber cure characteristics

The MR-502K 'Kwik Cure' magnetic rubber used for MRT inspections is a room temperature fast curing silicone rubber manufactured by Dynamold Inc.[*] According to the safety data safety for MR-502K [55], the rubber base consists of white silicone rubber containing a volume fraction of less than 1% black iron oxide particles. The curing of the rubber is initiated by adding small amounts of the catalysts stannous octoate and dibutyltin dilaurate. As the amount of catalysts required to achieve a particular cure rate are dependent on the ambient environment [56], the amounts are determined empirically at the time of inspection by performing a series of 'pot life' tests. The pot life, denoted $t_{PL}$, measures the time elapsed between addition of the catalysts and the time at which the cure process noticeably slows the flow of a stream of liquid rubber. In RAAF MRT inspections, $t_{PL,}$ is controlled via a requirement that it be between 5 and 6.5 min. Under these conditions, the rubber will have cured in approximately 15 min and may be removed from the component after approximately 30 min.

For reference, it is also noted that the term 'pot life' is not used consistently by all authors. Weltman *et al*. [57] use the term to describe the time taken for the kinematic viscosity of the magnetic rubber formulation to reach 3000 cStoke (equivalent to a dynamic viscosity of 30 Poise). This variation in definition has no bearing on the outcomes of the present work.

### 6.1.1 Viscometry

The cure kinetics for magnetic rubber MR-502K were examined using a cone and plate viscometer to measure the rubber viscosity as a function of time after the addition of the catalysts. In these experiments, the specimens consisted of 30 g of base rubber, with 0.06 g

---

[*] Dynamold, Inc. USA, www.dynamold.com/magrub.htm URL accessed 31 August 2012.

(2 drops) of dibutyltin dilaurate and 0.06 g (2 drops) of stannous octoate catalysts. The pot life of the magnetic rubber specimens was $t_{PL}$ = 5 min.

The results of the viscometry tests are plotted in Figure 15, from which it can be seen that for these samples, the viscosity increased linearly with time for approximately 300 s (5 min), followed by a more rapid increase. The results suggest that the pot life, as measured using the RAAF procedure, corresponds approximately to the time at which there is a deviation from the initial linear rate of change of viscosity.

A more extensive study (using rheological, spectroscopic and calorimetric techniques) would be able to firmly establish the precise relationship between pot life and the state of cure of the rubber. The requirements for rubber viscosity and cure, together with a discussion of the development of faster-curing rubber formulations and measurements of viscosity and sensitivity for a range of magnetic rubber formulations, can be found in the original MRT patents, and associated publications [3, 4, 46, 57].

From the viscosity measurements alone it is not possible to ascertain at what stage during cure the motion of the magnetic particles becomes sufficiently restricted that particle migration becomes ineffective. Such information is required to determine, for example, when a magnetising device could be removed without compromising the sensitivity of an inspection in progress. An indication of the time during which magnetic particle migration remains effective is provided by the series of experiments described below.
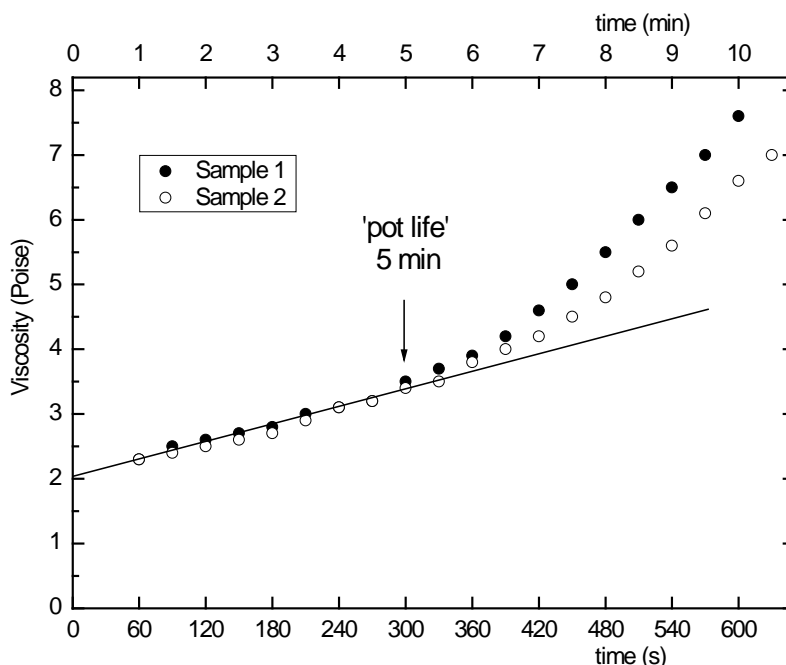


Figure 15. Viscosity as a function of time for samples of magnetic rubber during cure. The measured pot life of the samples was 5 min (arrowed).

### 6.1.2 Delayed Magnetisation

Experiments were performed in which the magnetic rubber was allowed to cure for different amounts of time prior to the initial application of the magnetic field. These experiments were intended to assist in the interpretation of the viscosity data presented in Figure 15 as well as to better determine when the retarding effects of rubber cure on particle mobility become greater than the magnetic force on the magnetic particles.

The cracks examined were 2.3 and 0.30 mm (0.090 and 0.012 inch) surface length fatigue cracks in the bore of one of the simulated mouse hole specimens used elsewhere in this report and in previous POD studies [5]. In this series of experiments, application of the magnetic field was delayed by 90, 150, 210, 270, 330, 390 or 450 s after the addition of catalysts to the base rubber. The magnetic field (70 G tangential) was then applied for 90 s using a DC electromagnet, with the pot life in this case being $t_{PL}$ = 390 s. Images of the resultant MRT silicone casts are displayed in Figure 16.

As is clear on inspection of Figure 16, the MRT indication for the smaller crack (length 0.30 mm or 0.012 inch) is no longer visible once application of the magnetic field is delayed by more than 270 s after mixing the catalysts with the base rubber. Thus, for a small crack, migration of magnetic particles to form MRT indications is ineffective well before the pot life of the rubber is reached. For the large crack (2.3 mm or 0.090 inch long), the strength of the MRT indication is gradually reduced as the post-mixing magnetisation delay is increased and beyond 270 s, only a very fine indication is present. This fine indication is thought to possibly arise from a weak residual magnetic flux density remaining in the specimen, even after AC demagnetisation, which for the large crack provides sufficient magnetic force on the particles to form a weak indication in the absence of the applied field.[*] These tests show that any significant particle movement leading to MRT crack indications has effectively ceased for $t > 0.6 \, t_{PL}$.



1 mm

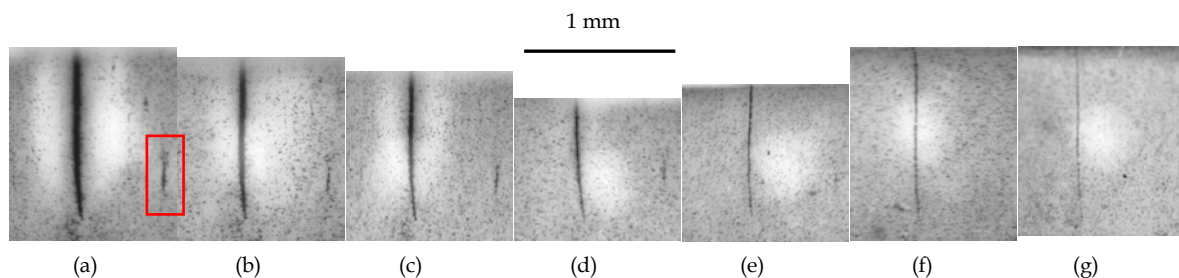| (a) | (b) | (c) | (d) | (e) | (f) | (g) |

*Figure 16. Variation in the appearance of MRT crack indications for bore cracks of length 2.3 and 0.30 mm (0.090 and 0.012 inch) due to delayed application of a magnetic field. Field applied for 90 s, with a post-mixing delay of (a) 90 s, (b) 150 s, (c) 210 s, (d) 270 s, (e) 330 s, (f) 390 s, and (g) 450 s. The pot life of this rubber mixture was 390 s. The 0.30 mm crack is outlined by the rectangle in (a).*

---

[*] These observations are consistent with earlier experimental trials conducted for DSTO in which a clear indication appeared for the 0.090 inch (2.3 mm) long crack with no externally applied field, and after the specimen had been demagnetised using a 50 Hz AC field. This indication was interpreted to be due to residual magnetisation remaining in the specimen after the AC demagnetisation. No indication was observed after the specimen was thoroughly demagnetised using an extremely low frequency (quasi-DC) field.

## 6.2 Magnetic particle size and shape

The size and shape of the magnetic particles in the rubber mixture were determined to give an increased understanding of the formation of MRT indications.

A sample of rubber cured without any magnetisation was examined under a scanning electron microscope. Figure 17 shows a sample of MR-502K rubber in which the magnetic particles (bright specks) are dispersed evenly throughout the rubber. A spectral analysis of the magnetic particles revealed the presence of magnetite within the silicone rubber base. Figure 18 shows the same sample at a higher magnification. Whilst a detailed particle size investigation was not undertaken, Figure 17 show the particles to be compact in shape (rather than needle - or platelike), with diameters of the order of 1–5 μm.

The observed particle size (< 10 μm) and compact shape is consistent with the required particle characteristics for the related 'wet method' of magnetic particle testing [12] and is also consistent with the preferred range of 0.8–10 μm stated in the 1978 General Dynamics patent [4]. The compact shape of the particles also implies that the magnetic permeability of the particle will be dominated by demagnetisation effects, so that the apparent relative permeability of an individual particle will be quite low ($\mu_r \sim 2$) [21] .
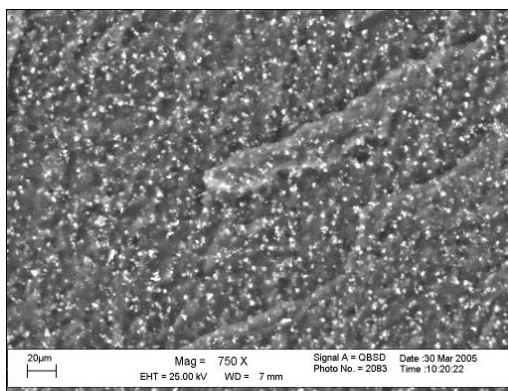


*Figure 17. Cured magnetic rubber MR-502K. The bright specks are the fine magnetite particles*
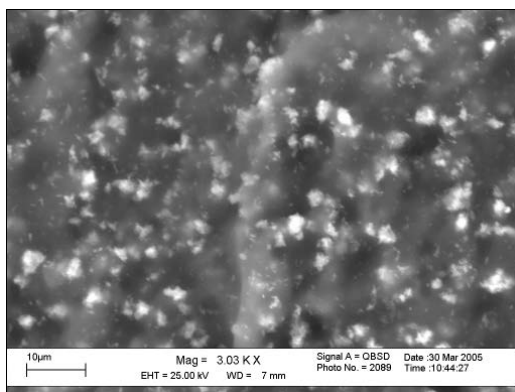


*Figure 18. Cured magnetic rubber MR-502K. The particle size is typically between 1 and 5 μm and particles tend to have a compact shape.*

# 7. Conclusions

This report draws together the results of a series of investigations aimed at resolving uncertainties concerning the reliability of active-field MRT of D6ac ultra high strength steel components.

In summary, this work has

- Developed and documented our current understanding of theoretical basis for MRT, including the forces acting on the magnetic particles within the rubber and the magnetisation state of a component during MRT.

- Established the relevant magnetic properties of D6ac steel for MRT purposes.

- Confirmed the basis for recommended magnetic field strengths to be applied for active-field MRT.

- Improved understanding of the effects of magnetic fields normal to the component surface on MRT indications, enabling reasonable limitations on normal magnetic fields for practical MRT to be defined.

- Investigated the degradation in sensitivity of active-field MRT for magnetisation conditions which depart from the optimum conditions in terms of the level of tangential or normal magnetic field.

- Investigated the effect of duration of magnetisation on MRT indications, as well as the effect of a delay in application of magnetisation during rubber cure.

This research has extended both the scientific understanding of the magnetic rubber testing process, and the available engineering data to underpin the application of MRT. The improved understanding of MRT may also benefit related magnetic inspection methods, such as MPI of welded structures.

# 8. Future Work

While the demand for underpinning science for MRT related to the F-111 has passed with the retirement of the fleet, gaps remain in the fundamental understanding of the MRT inspection technique. In niche areas, MRT continues to be an inspection option for steel structural and mechanical components in current aircraft. It is also possible that MRT will find applications to future aircraft if reliable inspections are required to detect very small surface-breaking cracks in critical steel structure.

On this basis, further research into active- and residual-field MRT of UHS steels, aimed at improved NDE capabilities for existing and future aircraft, would be useful. Such research would also potentially improve the sensitivity and reliability of MPI of critical welded

structures, with benefits for the fabrication and structural integrity management of maritime platforms.

Possible areas for future work include:

- High-precision measurement of the variation of residual leakage fields in the vicinity of fatigue cracks in UHS steels using magnetic force microscopy, allowing investigations of the flux leakage along the length of small or shallow fatigue cracks,

- Extension of the simple quantitative models described in Section 4.4 to support the future development of MRT and MPI with the aim of predicting the features (e.g. particle distribution, contrast) of crack indications. Such advanced models would require extension to 3-D, improved theoretical descriptions for magnetic leakage flux in the vicinity of a crack and would also need to incorporate the effects of varying viscosity and inter-particle interactions [43] into existing models for MPI [21, 42],

- Further experimental studies into the effect of varying the magnetisation duration with extension to cases in which two sequential orthogonal magnetisation directions are used during rubber cure, and

- Inspection reliability modelling to examine protocols for estimating $a_{NDI}$ in cases such as in Section 4, where the inspection parameters deviate from those values for which $a_{NDI}$ is well established.

# Acknowledgements

# References

[1]     Mills T, Clark G, Loader C, Sharp PK, and Schmidt R (2001), 'Review of F-111 Structural Materials', Defence Science and Technology Organisation, DSTO-TR-1118, Melbourne, Australia.

[2]     Hinders UA (July 20-22, 1970), 'F-111 Design Experience - Use of High Strength Steel' in *2nd Aircraft Design and Operations Meeting*, Los Angeles, CA, (American Institute of Aeronautics and Astronautics).

[3]     Weltman HJ, Carroll MT, Halkias JT, Kaarlela WT, and Reynolds JT, 'Method and Composition for Detecting Flaws in Metallic Surfaces, Holes and Otherwise', US Patent 3862047, (1975)

[4]     Weltman HJ, Carroll MT, Halkias JT, Kaarlela WT, and Reynolds JT, 'Castable Magnetic Particle Flaw Detection Composition and Method Using Constituents That Are Non-Volatile and Resistant to Oxidation Below 100 F and Having a Viscosity Less Than 12000 Centipoises', US Patent 4121157, (1978)

[5]     Harding CA and Hugo GR (2002), 'Experimental Determination of the Probability of Detection for Magnetic Rubber Inspections of F-111 Steel Components', Defence Science and Technology Organisation, DSTO–TN–0420, Melbourne, Australia.

[6]     Harding CA and Hugo GR (2001), 'Probability of Detection for Magnetic Rubber Inspections of F-111 Steel Components' in *Proceedings 10th Asia-Pacific Conference on NDT APCNDT*, Brisbane.

[7]     Burke SK and Ibrahim ME (2007), 'Restrictions on the Ratio of Normal to Tangential Field Components in Magnetic Rubber Testing', Defence Science and Technology Organisation, DSTO–TR–1991, Melbourne, Australia.

[8]     Burke SK and Ibrahim ME (2007), 'Electrical and Magnetic Properties of D6ac Steel', Defence Science and Technology Organisation, DSTO–TN–0757, Melbourne, Australia.

[9]     Ibrahim ME (2007), 'Limitations of Gaussmeters for the Measurement of Magnetic Fields in Magnetic Rubber Testing', Defence Science and Technology Organisation, DSTO–TN–0756, Melbourne, Australia.

[10]    Ibrahim ME and Burke SK (2007), 'Characterisation of Power Supply Units for Use in Central-Conductor Magnetic Rubber Testing', Defence Science and Technology Organisation, DSTO–TN–0753, Melbourne, Australia.

[11]    Burke SK, Ibrahim ME, and Hugo GR (2014), 'Principles and Application of Magnetic Rubber Testing for Crack Detection in High-Strength Steel Components: II. Residual-Field Inspection', Defence Science and Technology Organisation, DSTO–TR–3033, Melbourne, Australia.

[12]    Schmidt JT and Skeie K (1989), 'Magnetic Particle Testing' *Nondestructive Testing Handbook*; Vol. 6, 2nd ed., edited by McIntyre P (ASNT, New York, 1989)

[13]    Jiles D (1998), *Introduction to Magnetism and Magnetic Materials*, 2nd ed. (Chapman and Hall, London, 1998).

[14]    Beissner RE, Matzkanin GA, and Teller CM (1980), 'NDE Applications of Magnetic Leakage Field Methods: A State-of-the-Art Survey', NTIAC Southwest Research Institute, San Antonio, TX.

[15]    Blitz J (1991), *Electrical and Magnetic Methods of Nondestructive Testing* (IOP Publishing, Bristol, UK, 1991).

[16] Udpa SS (2007), 'Electromagnetic Testing' *Nondestructive Testing Handbook*; Vol. 5 (second printing), 3rd ed., edited by Moore PO (ASNT, Columbus OH, 2007)

[17] Lord W (1985), 'Applications of Numerical Field Modelling to Electromagnetic Methods of Nondestructive Testing' in *Electromagnetic Methods of Nondestructive Testing*; Vol. 3, edited by Lord W (Gordon and Breach, New York), p. 1–33.

[18] Förster F (1985), 'On the Way from the "Know-How" to the "Know-Why" in the Magnetic Leakage Field Method of Nondestructive Testing (Part One)', *Materials Evaluation* **43** 1154–1162.

[19] Förster F (1985), 'On the Way from the "Know-How" to the "Know-Why" in the Magnetic Leakage Field Method of Nondestructive Testing (Part Two)', *Materials Evaluation* **43** 1398–1404.

[20] Luborsky FE and Drummond BJ (1975), 'High Gradient Magnetic Separation: Theory Versus Experiment', *IEEE Transactions on Magnetics* **MAG-11** 1696–1700.

[21] Edwards C and Palmer SB (1986), 'The Magnetic Leakage Field of Surface-Breaking Cracks', *Journal of Physics D: Applied Physics* **19** 657–673.

[22] Stratton JA (1941), *Electromagnetic Theory* (McGraw-Hill, New York, 1941).

[23] Jackson JD (1999), *Classical Electrodynamics*, 3rd ed. (Wiley, New York, 1999).

[24] Zatsepin NN and Shcherbinin VE (1966), 'Calculation of the Magnetostatic Field of Surface Defects. I. Field Topography of Defect Models', *Defektoskopiya* **2** 50–59.

[25] Förster F (1982), 'Nondestructive Inspection by the Method of Magnetic Leakage Fields. Theoretical and Experimental Foundations of the Detection of Surface Cracks of Finite and Infinite Depth', *Soviet Journal of Nondestructive Testing* **11** 841–859.

[26] Sponder L, Athiniotis N, and Clark G (1992), 'Magnetic Leakage Field NDI Development for Aerospace Components', *Non-Destructive Testing Australia* **29** 133–136.

[27] Shur ML, Zagidulin RV, and Shcherbinin VE (1988), 'Theoretical Problems of the Formation of a Field of a Surface Defect', *Soviet Journal of Nondestructive Testing* **24** 153–163.

[28] Bowler JR and Bowler N (2002), 'Evaluation of the Magnetic Field near a Crack with Application to Magnetic Particle Inspection', *Journal of Physics D: Applied Physics* **35** 2237–2242.

[29] Lukyanets S, Snarskii A, Shamonin M, and Bakaev V (2003), 'Calculation of Magnetic Leakage Field from a Surface Defect in a Linear Ferromagnetic Material: An Analytical Approach', *NDT&E International* **36** 51–55.

[30] Minkov D, Lee J, and Shoji T (2000), 'Study of Crack Inversions Utilizing Dipole Model of a Crack and Hall Element Measurements', *Journal of Magnetism and Magnetic Materials* **217** 207–215.

[31] Mandache C and Clapham L (2003), 'A Model for Magnetic Flux Leakage Signal Predictions', *Journal of Physics D: Applied Physics* **36** 2427–2431.

[32] Zagidulin RV and Muzhitskii VF (2002), 'Three-Dimensional Model of Discontinuity Flaw of Finite Dimensions in a Ferromagnetic Plate', *Russian Journal of Nondestructive Testing* **38** 806–812.

[33] Shur ML, Zagidulin RV, and Shcherbinin VE (1987), 'Calculation of the Field of a Surface Flaw in a Nonlinear Ferromagnetic Medium', *Soviet Journal of Nondestructive Testing* **23** 69–74.

[34] Shur ML, Zagidulin RV, and Shcherbinin VE (1988), 'Self-Consistent Calculations of the Magnetostatic Field of the Surface Defect', *Defectoskopiya* **24** 3–13.

[35] Zagidulin RV and Shcherbinin VE (1991), 'Magnetic Field of a Surface Defect in a Ferromagnetic Plate', *Defectoskopiya* **27** 33–39.

[36] Zagiulin RV, Muzhitskii VF, and Kurozaev VP (1997), 'Calculation of the Magnetostatic Field of an Internal Defects in a Ferromagnetic Plate. I. ', *Russ. J. Nondestruct.* **33** 36-43.

[37] Zagidulin RV (1998), 'Calculation of the Remanent Magnetic Field of a Continuity Defect in a Ferromagnetic Article. I. The Magnetic Field inside a Ferromagnetic Material', *Russian Journal of Nondestructive Testing* **34** 717–726.

[38] Zagidulin RV (1998), 'Calculation of the Remanent Magnetic Field of a Continuity Defect in a Ferromagnetic Article. II. The Remanent Magnetic Field of a Defect in Air', *Russian Journal of Nondestructive Testing* **34** 727–773.

[39] Lord W, Bridges JM, Yen W, and Palanisamy R (1978), 'Residual and Active Leakage Fields around Defects in Ferromagnetic Materials' in *ASNT Spring Conference*, New Orleans, LA, (ASNT).

[40] Brudar B (1985), 'Magnetic Leakage Field Calculated by the Method of Finite Difference', *NDT International* **18** 353–357.

[41] McCoy JM and Tanner BK (1988), 'Simulation of Particle Trajectories in Magnetic Particle Inspection', *IEEE Transactions on Magnetics* **MAG-24** 1665–7.

[42] McCoy JM and Tanner BK (1990), 'Computer Simulations of Indications in Magnetic Particle Inspection', *Journal of Physics D: Applied Physics* **23** 593–599.

[43] Shelikhov GS (2004), 'The Effect of Coagulation of Magnetic Particles on the Detectability of Flaws in Magnetic-Powder Inspection', *Russian Journal of Nondestructive Testing* **40** 401–405.

[44] Hellier CJ (2001), *Handbook of Nondestructive Evaluation* (McGraw-Hill New York, 2001).

[45] Kifer II and Semenovskaya IB (1972), 'New Magnetic Particle Methods of Inspection', *Defectoskopiya* 41–45.

[46] Peck PM (2008), 'Magnetic Rubber' in *Magnetic Particle Testing*; Vol. 8, 3rd ed., edited by Moore DG (ASNT, Columbus, OH), p. 251–256.

[47] SAE (1999), 'Aerospace Material Specification - Inspection Process, Magnetic Rubber', SAE Aerospace, AMS-I-83387, USA.

[48] RAAF (2012), 'MRT/GEN/1 - Magnetic Rubber Testing' in *AAP 7002.043-36 Non-Destructive Testing General Procedures* (Royal Australian Air Force, Nondestructive Testing Standards Laboratory).

[49] Lord W and Oswald DJ (1972), 'Leakage Field Methods of Defect Detection', *International Journal of Nondestructive Testing* **4** 249–274.

[50] Stanley RK (1985), 'Basic Principles of Magnetic Flux Leakage Inspection Systems for Evaluation of Oil Country Tubular Goods' in *Electromagnetic Methods of Nondestructive Testing*; Vol. 3, edited by Lord W (Gordon and Breach Science Publishers, London), p. 97.

[51] Oehl CL and Swartzendruber LJ (1982), 'On the Optimum Applied Field for Magnetic Particle Inspection Using Direct Current', *Journal of Nondestructive Evaluation* **3** 125–136.

[52] BS EN ISO 9934-1:2001 'Method for Magnetic Particle Flaw Detection', British Standard, UK

[53]    Shelikhov GS (2004), 'Dependence of the Detectability of Flaws on the Distribution of the Magnetizing Field in the Vicinity of a Flaw', *Russian Journal of Nondestructive Testing* **40** 397–400.

[54]    Smistrup K, Hansen O, Bruss H, and Hansen MF (2005), 'Magnetic Separation in Microfluidic Systems Using Microfabricated Electromagnets - Experiments and Simulations', *Journal of Magnetism and Magnetic Materials* **293** 597–604.

[55]    Dynamold (2003), 'Material Safety Data Sheet MR-502K Magnetic Rubber Inspection Material ', http://www.dynamold.com/pdf_files/502c.pdf, (Date accessed, 6 Dec 2007).

[56]    Wilson L (1977), 'The Influence of Catalyst Concentration and Temperature on the Curing Time of Magnetic Rubber', Defence Science and Technology Organisation, Materials Note 117, Melbourne, Australia.

[57]    Weltman HJ, Kaarlela WT, Reynolds JD, and Halkias JE (1984), 'Development and Applications of Fast-Sensitive Magnetic Rubber Inspection Formulations', *Materials Evaluation* **42** 917–921.

# Appendix A: MRT Normal-to-Tangential Field Trial

## A.1. Matrix of experimental results

As described in Section 4, a matrix of experiments was designed in which both the tangential and normal field components were varied in order to estimate the POD for a wide range of MRT field parameters. MRT pours were performed using six mouse hole-type representative specimens used in a previous POD trial [5]. The largest three cracks on the bore surface of each of the mouse hole specimens were investigated, giving a range of crack lengths between 0.15 and 2.3 mm (0.006 and 0.090 inch). The specimen designation and the lengths of the cracks, as determined by master crack inspections under load, together with a summary of the results are presented in Tables A1–A3. Each Table corresponds to one of the three chosen tangential fields.

For each field condition in Tables A1–A3, a notional POD value has been assigned to the crack indication using a scale of 0 to 1 in units of 0.1 based on a collective assessment by DSTO staff experienced with MRT of the appearance and strength of the crack indications. Note, in some cases a crack length is reported where POD = 0 is assigned. This is because the crack would have been missed in a regular inspection, but with prior knowledge of the crack location it was possible to estimate the crack length.

For comparison, the estimated value from the 2001 MRT POD trial [5] is $a_{90/95}$ = 0.30 mm (0.012 inch).

The inspection procedure is given in Appendix B.

*Table A1. Summary of results for MRT Normal-Tangential Field Trials: 27 G Tangential Field. The crack length is the length on the surface of the bore. Crack types: C = corner crack; B = bore crack; MOC = multiple-origin cracking. The strength of the indications is ranked using the colour code given in the Legend below. The numbers that appear in the strength column are the difference between the measured crack length and the true length (in units of 0.001 inch). The method for assigning a POD to each crack is described in §4.2.*

| $B_t$ (G) | Coupon | Crack Length (inch) | Crack Type | Ratio $B_n:B_t$ 0:1 | | | 1:1 | | | 2:1 | | | 3:1 | | |
|---|---|---|---|---|---|---|---|---|---|---|---|---|---|---|---|
| | | | | Measured crack length inch | Strength | POD | Measured crack length inch | Strength | POD | Measured crack length inch | Strength | POD | Measured crack length inch | Strength | POD |
| | EL14AB1 | 0.090 | C | 0.084 | -6 | 1.0 | 0.080 | -10 | 1.0 | 0.087 | -3 | 1.0 | 0.070 | -20 | 1.0 |
| | EL6AD3 | 0.054 | B | 0.049 | -5 | 1.0 | | | 1.0 | 0.051 | -3 | 1.0 | 0.046 | -8 | 1.0 |
| | EL4AE3 | 0.043 | B | 0.044 | 1 | 1.0 | | | 1.0 | 0.040 | -3 | 1.0 | 0.038 | -5 | 1.0 |
| | EL17AB1 | 0.025 | C | 0.028 | 3 | 1.0 | | | 1.0 | 0.028 | 3 | 1.0 | 0.024 | -1 | 0.9 |
| | EL3AF3 | 0.013 | MOC | 0.013 | 0 | 1.0 | 0.014 | 1 | 1.0 | 0.011 | -2 | 1.0 | – N – | | 0.0 |
| 27 ± 1 | EL14AB1 | 0.012 | B | 0.011 | -1 | 1.0 | 0.009 | -3 | 0.9 | 0.013 | 1 | 0.8 | 0.014 | 2 | 0.0 |
| | EL3AF3 | 0.011 | MOC | 0.010 | -1 | 1.0 | 0.006 | -5 | 0.9 | 0.006 | -5 | 0.9 | – N – | | 0.0 |
| | EL16AC1 | 0.010 | C | 0.009 | -1 | 1.0 | 0.009 | 0 | 0.9 | – N – | | 0.0 | 0.011 | 1 | 0.0 |
| | EL3AF3 | 0.009 | MOC | 0.007 | -2 | 1.0 | 0.008 | -1 | 0.9 | – N – | | 0.5 | – N – | | 0.0 |
| | EL14AB1 | 0.008 | B | 0.007 | -1 | 0.9 | 0.007 | -1 | 0.8 | 0.009 | 1 | – X – | 0.005 | -3 | 0.0 |
| | EL4AE3 | 0.006 | B | 0.007 | 1 | 1.0 | | | 0.0 | 0.004 | -2 | 0.0 | – N – | | 0.0 |

No measurement performed but POD result assigned

– N –   No crack length measurement possible

– X –   No POD estimate made

"Strong" - indication clearly highlighted against background, correctly predicts length
'Weak' - indication reasonably highlighted against background but somewhat unclear
'Marginal' - indication shows location of crack but sizing not possible
'Not visible' - indication either not present or not expected to be detected at all
'Not performed' - No measurement performed

*Table A2.   Summary of results for MRT Normal-Tangential Field Trials: 20 G Tangential Field. The crack length is the length on the surface of the bore. Crack types: C = corner crack; B = bore crack; MOC = multiple-origin cracking. The strength of the indications is ranked using the colour code given in the Legend below. The numbers which appear in the strength column are the difference between the measured crack length and the true length (in units of 0.001 inch). The method for assigning a POD to each crack is described in §4.2.*

| $B_t$ (G) | Coupon | Crack Length (inch) | Crack Type | Ratio $B_n$:$B_t$ | | | | | | | | | | | | |
|---|---|---|---|---|---|---|---|---|---|---|---|---|---|---|---|
| | | | | 0:1 | | | 1:1 | | | 2:1 | | | 3:1 | | |
| | | | | Measured crack length inch | Strength | POD | Measured crack length inch | Strength | POD | Measured crack length inch | Strength | POD | Measured crack length inch | Strength | POD |
| | EL14AB1 | 0.090 | C | 0.086 | -4 | 1.0 | 0.079 | -11 | 1.0 | 0.082 | -8 | 1.0 | 0.084 | -6 | 1.0 |
| | EL6AD3 | 0.054 | B | 0.048 | -6 | 1.0 | 0.047 | -7 | 1.0 | 0.049 | -5 | 0.9 | 0.051 | -3 | 1.0 |
| | EL4AE3 | 0.043 | B | 0.041 | -2 | 1.0 | 0.039 | -4 | 1.0 | 0.039 | -4 | 1.0 | 0.041 | -2 | 1.0 |
| | EL17AB1 | 0.025 | C | 0.027 | 2 | 1.0 | 0.024 | -1 | 1.0 | 0.024 | -1 | 1.0 | 0.027 | 2 | 1.0 |
| | EL3AF3 | 0.013 | MOC | 0.013 | 0 | 1.0 | 0.011 | -2 | 1.0 | 0.013 | 0 | 1.0 | 0.010 | -3 | 0.8 |
| 20 ± 1 | EL14AB1 | 0.012 | B | 0.012 | 0 | 0.8 | 0.009 | -3 | 0.5 | 0.010 | -2 | 0.0 | 0.011 | -1 | 0.3 |
| | EL3AF3 | 0.011 | MOC | 0.008 | -3 | 1.0 | 0.006 | -5 | 0.7 | 0.005 | -6 | 0.9 | 0.009 | -2 | 0.2 |
| | EL16AC1 | 0.010 | C | 0.004 | -6 | 0.9 | 0.005 | -5 | 0.6 | – N – | | 0.3 | 0.007 | -3 | 0.4 |
| | EL3AF3 | 0.009 | MOC | 0.007 | -2 | 1.0 | 0.007 | -2 | 0.8 | 0.008 | -1 | 0.7 | – N – | | 0.0 |
| | EL14AB1 | 0.008 | B | 0.006 | -2 | 0.5 | 0.008 | 0 | 0.6 | 0.008 | 0 | 0.1 | 0.006 | -2 | 0.2 |
| | EL4AE3 | 0.006 | B | – N – | | 0.0 | – N – | | 0.3 | 0.005 | -1 | 0.6 | 0.008 | 2 | 0.4 |

|  | No measurement performed but POD result assigned |
|---|---|
| – N – | No crack length measurement possible |
| – X – | No POD estimate made |

| | |
|---|---|
| | 'Strong' - indication clearly highlighted against background, correctly predicts length |
| | 'Weak' - indication reasonably highlighted against background but somewhat unclear |
| | 'Marginal' - indication shows location of crack but sizing not possible |
| | 'Not visible' - indication either not present or not expected to be detected at all |
| | 'Not performed' - No measurement performed |

Table A3. *Summary of results for MRT Normal-Tangential Field Trials: 16 G Tangential Field. The crack length is the length on the surface of the bore. Crack types: C = corner crack; B = bore crack; MOC = multiple-origin cracking. The strength of the indications is ranked using the colour code given in the Legend below. The numbers which appear in the strength column are the difference between the measured crack length and the true length (units 0.001 inch). The method for assigning a POD to each crack is described in §4.2.*

| $B_t$ (G) | Coupon | Crack Length (inch) | Crack Type | Ratio $B_n:B_t$ | | | | | | | | | | | | | | | |
| | | | | 0:1 | | | 1:1 | | | 2:1 | | | 3:1 | | | 4:1 | | |
| | | | | Measured crack length inch | Strength | POD | Measured crack length inch | Strength | POD | Measured crack length inch | Strength | POD | Measured crack length inch | Strength | POD | Measured crack length inch | Strength | POD |
| | EL14AB1 | 0.090 | C | 0.084 | -6 | 1.0 | 0.078 | -12 | 1.0 | 0.086 | -4 | 1.0 | 0.080 | -10 | 1.0 | 0.083 | -7 | 1.0 |
| | EL6AD3 | 0.054 | B | 0.050 | -4 | 1.0 | 0.045 | -9 | 1.0 | 0.044 | -10 | 1.0 | 0.047 | -7 | 1.0 | 0.045 | -9 | 1.0 |
| | EL4AE3 | 0.043 | B | 0.037 | -6 | 1.0 | 0.037 | -6 | 1.0 | 0.039 | -4 | 1.0 | 0.042 | -1 | 1.0 | 0.039 | -4 | 0.8 |
| | EL17AB1 | 0.025 | C | 0.027 | 2 | 1.0 | 0.026 | 1 | 1.0 | 0.026 | 1 | 1.0 | 0.025 | 0 | 1.0 | 0.027 | 2 | 0.9 |
| | EL3AF3 | 0.013 | MOC | 0.011 | -2 | 0.5 | 0.012 | -1 | 0.9 | 0.010 | -3 | 0.6 | – N – | | 0.0 | | | 0.0 |
| 16 ± 1 | EL14AB1 | 0.012 | B | 0.011 | -1 | 0.7 | 0.007 | | 0.0 | 0.014 | 2 | 0.1 | 0.009 | -3 | 0.2 | – N – | | 0.1 |
| | EL3AF3 | 0.011 | MOC | 0.009 | -2 | 0.3 | 0.006 | -5 | 0.5 | 0.008 | -3 | 0.2 | – N – | | 0.0 | | | 0.0 |
| | EL16AC1 | 0.010 | C | 0.006 | -4 | 0.9 | 0.006 | -4 | 0.8 | 0.005 | -5 | 0.2 | – N – | | 0.0 | – N – | | 0.0 |
| | EL3AF3 | 0.009 | MOC | 0.005 | -4 | 0.0 | 0.007 | -2 | 0.3 | 0.007 | -2 | 0.0 | – N – | | 0.0 | | | 0.0 |
| | EL14AB1 | 0.008 | B | 0.006 | -2 | 0.7 | 0.010 | 2 | 0.0 | 0.003 | -5 | 0.0 | 0.006 | -2 | 0.0 | 0.005 | -3 | 0.0 |
| | EL4AE3 | 0.006 | B | – N – | | 0.2 | – N – | 1 | 0.0 | 0.006 | | 0.0 | 0.007 | | 0.0 | – N – | | 0.0 |

 No measurement performed but POD result assigned

– N –  No crack length measurement possible

– X –  No POD estimate made

 'Strong' - indication clearly highlighted against background, correctly predicts length
 'Weak' - indication reasonably highlighted against background but somewhat unclear
 'Marginal' - indication shows location of crack but sizing not possible
 'Not visible' - indication either not present or not expected to be detected at all
 'Not performed' - No measurement performed

# Appendix B: Inspection Procedure

The following inspection procedure was used for the experimental trials described in Section 4 and Appendix A. This procedure is closely related to the procedure MRT NORMAL/TANGENTIAL FIELD MEASUREMENTS reproduced in DSTO-TR-1991 [7].

# MRT NORMAL/TANGENTIAL FIELD MEASUREMENTS
# (SECOND SERIES OF EXPERIMENTS)

## INTRODUCTION

9. **Operator Level. II**

10. **Method. MRT**

11. **Applicability. Mousehole Test Specimens**

12. **MRN. Various**

13. **Material. D6ac Steel**

### NOTE

This Specific Procedure shall be used in conjunction with a General Procedure. Only information that emphasises, differs from, or is additional to the requirements of the General Procedure is included. All other procedural steps shall be performed in accordance with the General Procedure. The information laid down in this procedure takes precedence over the General Procedure.

14. Reference Document. **This procedure is to be used in conjunction with AAP 7002.043-36 Sect 4 Chap 2 (MRT/GEN/1).**

### PURPOSE

15. **The purpose of this test is to observe the properties of a Magnetic Rubber indication under varying conditions of applied tangential magnetic field, and normal to tangential field ratio, applied to cracks in mousehole specimens. Experiments at different combinations of tangential field strength and normal:tangential field ratios are to be performed in accordance with a defined test matrix.**

### EQUIPMENT REQUIREMENTS

16. **The following equipment is required:**

    16.1 **Powershoe magnet including pole pieces and suitable bridging (dampening) shims.**

    16.2 **Gaussmeter with transverse probe.**

    16.3 **Parker magnetising yoke.**

    16.4 **Gauss measuring guide.**

    16.5 **Dummy specimen EL17AF1 (for setting up correct magnetic field strength).**

    16.6 **Test matrix specifying combinations of tangential and normal field strengths and specimen numbers to be used for each test.**
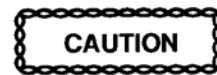
    16.7 **Specimens as specified in test matrix.**

    16.8 **Additional equipment as detailed in MRT/GEN/1.**

### SAFETY PRECAUTIONS

17. **As per MRT/GEN/1.**

### PRE-TEST REQUIREMENTS

```
CAUTION
```

D6AC STEEL COMPONENTS SHALL NOT BE LEFT IN AN UNINHIBITED CONDITION FOR OVER ONE HOUR. COAT UNINHIBITED COMPONENTS WITH THE APPROVED CORROSION INHIBITER, OR CORROSION WILL RESULT.

### MAGNET POSITIONS

18. **Casts will be poured and measurements performed for three different orientations of the magnet assembly:**

    18.1 **Position 1 (refer to Figure B3-Figure B5). The measured tangential field should be as specified in the test matrix, and the measured normal field should be less than 5 gauss.**

    18.2 **Position 2 (refer to Figure B6). Rotate the magnet assembly to**

40

achieve a normal-to-tangential field ratio of 1:1, 2:1 or 3:1 as specified in the test matrix. The target gauss levels for each direction are specified in the test matrix.

18.3 **Position 3 (refer to Figure B7).** Rotate the magnet assembly in the opposite direction to (18.2) to achieve a normal-to-tangential field ratio of -1:1, -2:1 or -3:1 as specified in the test matrix. The target gauss levels for each direction are specified in the test matrix.

19. **For test matrix columns 1:1, 2:1 and 3:1, pours and measurements are required for both magnet positions 2 and 3.**

## EQUIPMENT SETTINGS/SET-UP PROCEDURE

### NOTES

- This DC demagnetisation is to be performed on each specimen *before the first experiments*.

- This DC demagnetisation is to be repeated *whenever the applied tangential field strength is to be reduced* for a specimen from a previous higher value.

20. **Each test specimen (including the dummy specimen EL17AF1) is to be DC demagnetised as follows:**

20.1 **continuously rotate the specimen within a DC field whilst the DC field strength is gradually reduced to zero (for example by moving the source of the DC field away from the specimen whilst the specimen is rotating). The specimen rotation is to be about either the specimen width direction or the specimen thickness direction and the magnetic field is to be normal to the rotation axis.**

### NOTE

The location of the cracks relative to the mousehole will be marked on the specimens.

20.2 **Using the Gaussmeter transverse probe, measure the normal and tangential field in the vicinity of the crack and the normal field at the ends of the specimen, and ensure all measured fields are less than 2 gauss. If not, repeat from 20a.**

21. **Carry out the set-up procedure in accordance with MRT/GEN/1 and the following:**

21.1 **Apply the Parker yoke to the face of the specimen containing the crack.**

21.2 **Select the AC setting on the yoke.**

21.3 **Energise the yoke, and remove from specimen while energised in order to demagnetise the specimen.**

21.4 **Using the Gaussmeter transverse probe, measure the normal and tangential field in the vicinity of the crack and the normal field at the ends of the specimen, and ensure all measured fields are less than 2 gauss. If not, repeat from 21.1.**

21.5 **Repeat paragraph 21.1-21.4 for dummy specimen EL17AF1.**

21.6 **Repeat paragraph 21.1-21.5 for all measurements.**

## TEST PROCEDURE

22. **Carry out the test in accordance with the MRT/GEN/1 and the following:**

22.1 **Insert the gauss measurement guide into the mousehole of the dummy specimen EL17AF1, taking care that the measurement location coincides with the crack location (ref. Figure ).**

22.2 **Apply the magnet assembly to the specimen, in the required Position 1, 2 or 3 (ref. Figure B3-Figure B7).**

### NOTE

Install/remove gauss damping shims as required, to control the overall magnetic field strength.

**22.3** **Insert the transverse Gaussmeter probe into the gauss measurement guide, and adjust magnet assembly to achieve the required tangential and normal field readings for the relevant position, as specified in the test matrix. (An example test matrix is shown in Table 1).**

**22.4** **Remove gauss measurement guide and magnet assembly from dummy specimen, taking care not to disturb magnet assembly.**

**22.5** **Select and prepare the required test specimen.**

**22.6** **If the required tangential field strength is lower than a previously used value for this specimen, DC demagnetise the specimen IAW paragraph 20.1 to 0.**

**NOTE**

To enable correct orientation of the probe guide, the location of the cracks relative to the mousehole will be marked on the specimens. **It is essential that the gauss measurement location correctly coincides with the crack location.**

**22.7** **Insert the gauss measurement guide into the mousehole of the test specimen, taking care that the measurement location coincides with the crack location (ref. Figure ).**

**22.8** **Apply the magnet assembly to the specimen, in the required Position 1, 2 or 3 (ref. Figure B3-Figure B7).**

**NOTES**

- Small adjustments to magnet position are permitted to achieve the required fields.

- If changes to the number of gauss damper shims are required,. repeat the setup on the dummy specimen, paragraphs 22.1 to 22.9.

- If the tangential field overshoots the target value by more than 4 gauss, specimen must be DC demagnetised before proceeding.

**22.9** **Insert the transverse Gaussmeter probe into the gauss measurement guide, and adjust magnet assembly to achieve the required tangential and normal field readings for the relevant position, as specified in the test matrix.**

22.9.1 If the measured tangential field overshoots the target value by more than 4 gauss, DC demagnetise the specimen IAW paragraph 20.1 to 0 then repeat paragraph 22.9.

22.9.2 If the required tangential and normal fields cannot be achieved without changing the number of gauss damper shims, repeat paragraphs 22.1 to 22.9.

**22.10** **Record both the tangential and normal field values.**

**22.11** **Remove gauss measurement guide, taking care not to disturb magnet assembly.**

**NOTE**

The digit in the magnet position code refers to the normal:tangent field ratio as 0 (normal field <5G), 1, 2, 3 etc. The + or – sign indicates whether the magnet was rotated to position 2 (+) or position 3 (-)..

**22.12** **Prepare identification tag to be inserted into rubber before it cures. Tag should be labelled with: Specimen number, magnet position (N0, N1+, N1-, N2+, or N2- etc), pour number and date. e.g. "EL3AC1 N1+ #2 2/2/07"**

**22.13** **Build dam around mousehole, and pour pre-determined magnetic rubber mixture.**

**22.14** **Gently insert identification tag into top of rubber before it cures.**

**22.15** **Remove the cured cast and place it into a re-sealable plastic bag, suitably identified with the specimen number, magnet assembly position,**

**levels of normal and tangential field, and date of test.**

**22.16 Examine each cast under low magnification. Photograph and measure the length of relevant indications at consistent levels of magnification. Include scaling bars. Also report the clarity of all indications using descriptions such as: not visible, barely visible, fuzzy, indistinct, clear, strong, very strong.**

**22.17 Demagnetise specimen IAW paragraph 21.**

**22.18 Repeat paragraph 22.1 to 22.17 for all measurements.**

## POST-TEST REQUIREMENTS

**23. Demagnetise specimen using magnetising yoke as per paragraph 21. Apply corrosion inhibitor to mousehole region of specimen.**

## REPORTING

**24. A report is to be prepared which includes:**

**24.1 photographs of all indications, including scale markers.**

**24.2 measured size of all indications.**

**24.3 a description of the strength or clarity of all indications using descriptors such as not visible, barely visible, fuzzy, indistinct, clear, strong, very strong.**

**24.4 Any required or inadvertent deviations from this procedure.**

**24.5 Any other observations which may assist in interpreting the results or planning future experiments.**

*Table B1 Example Test Matrix*

| Tangential Field Strength ($H_t$) | Normal to tangential field ratio ($H_n$ = required normal field strength) | | | |
|---|---|---|---|---|
| | **Zero** | **1:1** | **2:1** | **3:1** |
| 27 ± 1 gauss | $H_n$ < 5 gauss<br><br>Specimens:<br><br>XXnnXXn<br><br>XXnnXXn | $H_n$: 27 ± 3 gauss<br><br>Specimens:<br><br>XXnnXXn | $H_n$: 55 ± 5 gauss<br><br>Specimens:<br><br>XXnnXXn | $H_n$: 80 ± 8 gauss<br><br>Specimens:<br><br>XXnnXXn |
| 20 ± 1 gauss | $H_n$ < 5 gauss<br><br>Specimens:<br><br>XXnnXXn | $H_n$: 20 ± 2 gauss<br><br>Specimens:<br><br>XXnnXXn | $H_n$: 40 ± 4 gauss<br><br>Specimens: | $H_n$: 60 ± 6 gauss<br><br>Specimens: |
| 16 ± 1 gauss | $H_n$ < 5 gauss<br><br>Specimens:<br><br>XXnnXXn | $H_n$: 16 ± 2 gauss<br><br>Specimens: | $H_n$: 32 ± 3 gauss<br><br>Specimens: | $H_n$: 48 ± 5 gauss<br><br>Specimens: |
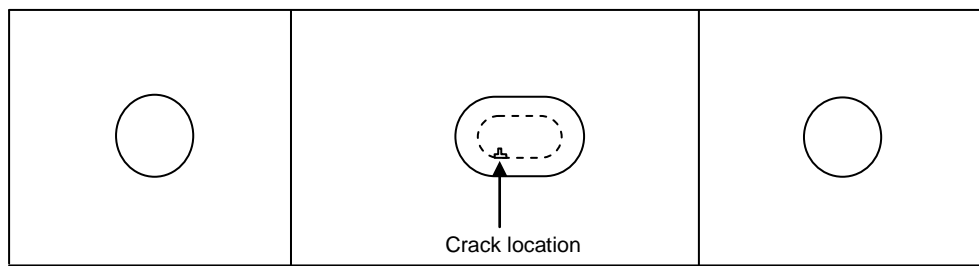
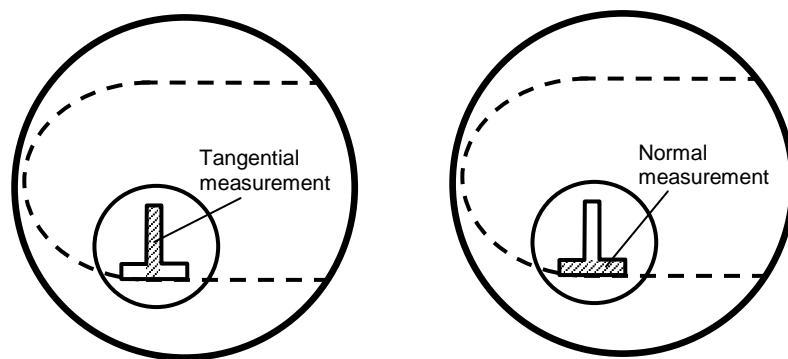*Figure B1. Mousehole specimen, gauss measurement guide inserted in mousehole*



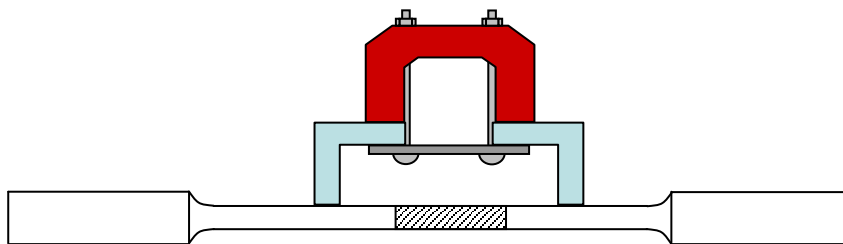*Figure B2. Detail of gauss measurement guide, showing probe tip orientation (thatched)*



*Figure B3. Magnet assembly applied to specimen in position 1. The assembly is progressively rotated to achieve the required normal and tangential field levels.*
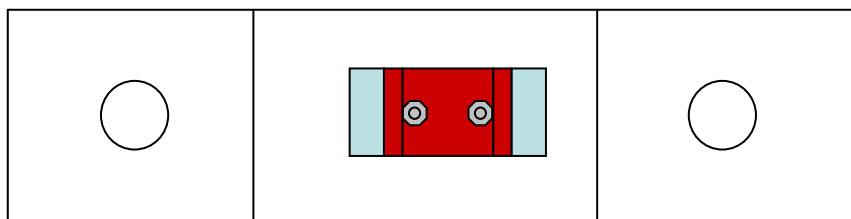


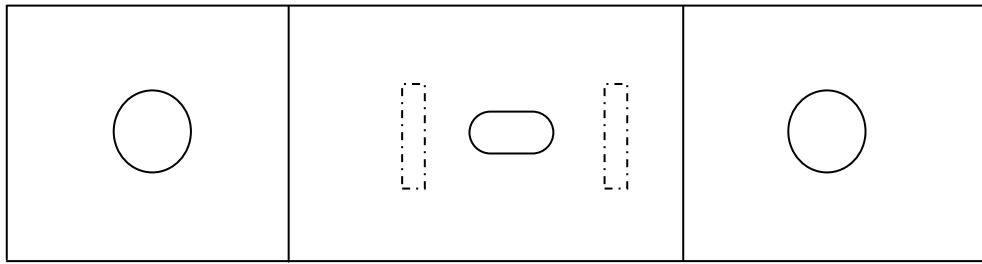*Figure B4. Plan view of magnet assembly applied to specimen in position 1*

*Figure B5. Position 1. Feet of pole pieces shown (dashed line) in relation to mousehole. Tangential field level is 25-30 gauss, and normal field level is maximum 5 gauss.*
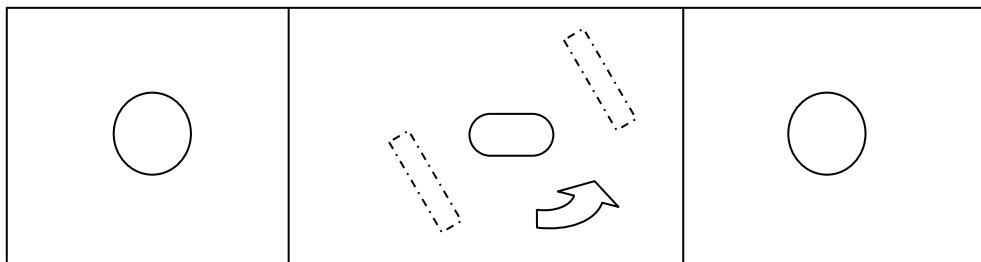


*Figure B6. Position 2. The magnet assembly is rotated about the centre of the mousehole, to achieve a normal-to-tangential field ratio of 1:1. Target field level is 25 – 30 gauss.*
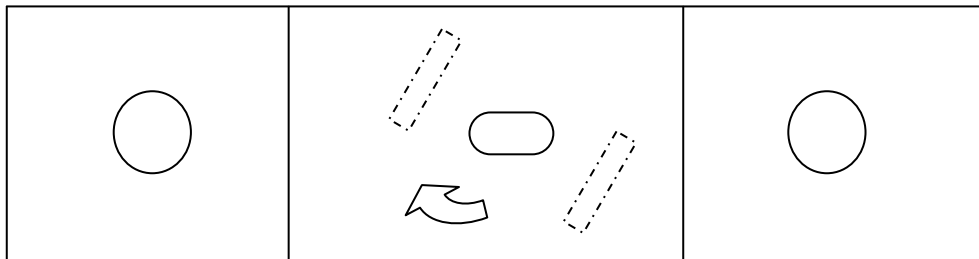


*Figure B7. Position 3. Rotate magnet assembly in opposite direction to Position 2, to achieve a normal-to-tangential field ratio of -1:1. Target field level is ± (25 to 30) gauss.*

| DEFENCE SCIENCE AND TECHNOLOGY ORGANISATION DOCUMENT CONTROL DATA | | 1. PRIVACY MARKING/CAVEAT (OF DOCUMENT) |
|---|---|---|

| 2. TITLE<br><br>Principles and Application of Magnetic Rubber Testing for Crack Detection in High-Strength Steel Components: I. Active-Field Inspection | 3. SECURITY CLASSIFICATION (FOR UNCLASSIFIED REPORTS THAT ARE LIMITED RELEASE USE (L) NEXT TO DOCUMENT CLASSIFICATION)<br><br>Document      (U)<br>Title          (U)<br>Abstract     (U) |
|---|---|

| 4. AUTHOR(S)<br><br>S K Burke, M E Ibrahim and G R Hugo | 5. CORPORATE AUTHOR<br><br>Defence Science and Technology Organisation<br>506 Lorimer St<br>Fishermans Bend Victoria 3207 Australia |
|---|---|

| 6a. DSTO NUMBER<br>DSTO-TR-3032 | 6b. AR NUMBER<br>AR-016-112 | 6c. TYPE OF REPORT<br>Technical Report | 7. DOCUMENT DATE<br>December 2014 |
|---|---|---|---|

| 8. FILE NUMBER<br>2012/1174319/1 | 9. TASK NUMBER<br>AIR 07/101 | 10. TASK SPONSOR<br>DGTA-ADF | 11. NO. OF PAGES<br>46 | 12. NO. OF REFERENCES<br>57 |
|---|---|---|---|---|

| 13. DSTO Publications Repository<br><br>http://dspace.dsto.defence.gov.au/dspace/ | 14. RELEASE AUTHORITY<br><br>Chief, Maritime Division |
|---|---|

15. SECONDARY RELEASE STATEMENT OF THIS DOCUMENT

*Approved for public release*

OVERSEAS ENQUIRIES OUTSIDE STATED LIMITATIONS SHOULD BE REFERRED THROUGH DOCUMENT EXCHANGE, PO BOX 1500, EDINBURGH, SA 5111

16. DELIBERATE ANNOUNCEMENT

No Limitations

| 17. CITATION IN OTHER DOCUMENTS | Yes |
|---|---|

18. DSTO RESEARCH LIBRARY THESAURUS  http://web-vic.dsto.defence.gov.au/workareas/library/resources/dsto_thesaurus.shtml

magnetic rubber testing, measurement, magnetic fields, fatigue cracks, detection, steel, F-111 aircraft

19. ABSTRACT
Magnetic rubber testing (MRT) is a sensitive non-destructive inspection technique, capable of detecting cracks as small as 0.5 mm (0.020 inch) in length with high reliability. Since its introduction in the 1970s, MRT has been successfully used to inspect high-strength steel aerospace components for surface-breaking fatigue cracks. However, despite its widespread use and apparent simplicity, the underpinning science of MRT is not highly developed. In response to some uncertainties regarding potential unreliability in the application of MRT for certain test conditions, the scientific principles governing both active-field and residual-field variants of MRT were examined. The results of theoretical and experimental investigations into active-field MRT are documented in the current report, which describes the principles of active-field MRT, and then examines both the basis for verification of adequate applied field strength for D6ac steel and the effect of the perpendicular versus tangential components of applied magnetic field on inspection reliability. The results of related study into residual-field MRT are presented in a companion DSTO report.